General second-order covariance of Gaussian maximum likelihood estimates applied to passive source localization in fluctuating waveguides

Ioannis Bertsatos
Department of Mechanical Engineering, Massachusetts Institute of Technology, Cambridge, Massachusetts 02139

Michele Zanolin
Department of Physics, Embry-Riddle Aeronautical University, Prescott, Arizona 86301

Purnima Ratilal
Department of Electrical and Computer Engineering, Northeastern University, Boston, Massachusetts 02115

Tianrun Chen
Department of Earth and Planetary Sciences, Massachusetts Institute of Technology, Cambridge, Massachusetts 02139

Nicholas C. Makris[a)]
Department of Mechanical Engineering, Massachusetts Institute of Technology, Cambridge, Massachusetts 02139

(Received 25 January 2010; revised 6 July 2010; accepted 10 August 2010)

A method is provided for determining necessary conditions on sample size or signal to noise ratio (SNR) to obtain accurate parameter estimates from remote sensing measurements in fluctuating environments. These conditions are derived by expanding the bias and covariance of maximum likelihood estimates (MLEs) in inverse orders of sample size or SNR, where the first-order covariance term is the Cramer-Rao lower bound (CRLB). Necessary sample sizes or SNRs are determined by requiring that (i) the first-order bias and the second-order covariance are much smaller than the true parameter value and the CRLB, respectively, and (ii) the CRLB falls within desired error thresholds. An analytical expression is provided for the second-order covariance of MLEs obtained from general complex Gaussian data vectors, which can be used in many practical problems since (i) data distributions can often be assumed to be Gaussian by virtue of the central limit theorem, and (ii) it allows for *both* the mean and variance of the measurement to be functions of the estimation parameters. Here, conditions are derived to obtain accurate source localization estimates in a fluctuating ocean waveguide containing random internal waves, and the consequences of the loss of coherence on their accuracy are quantified.
 [DOI: 10.1121/1.3488303]

PACS number(s): 43.30.Pc, 43.60.Jn, 43.30.Re, 43.60.Gk [WMC] Pages: 2635–2651

I. INTRODUCTION

In remote sensing applications, parameter estimation often requires the nonlinear inversion of measured data that are randomized by additive signal-independent ambient noise, as well as signal-dependent noise arising from fluctuations in the propagation medium. Parameter estimates obtained from such nonlinear inversions are typically biased and do not attain desired experimental error thresholds. For this reason, necessary conditions have been developed on sample size or signal to noise ratio (SNR) to obtain accurate estimates and aid experimental design.[1]

These conditions are derived by first expanding the bias and covariance of maximum likelihood estimates (MLEs) in inverse order of sample size or SNR, where the first-order covariance term is the minimum variance, the Cramer-Rao lower bound (CRLB), which is also the minimum mean square error (MSE) of any unbiased estimate regardless of the method of estimation. It is then required that (i) the first-order bias term and the second-order covariance term become much smaller than the true value of the parameter and the CRLB, respectively, and (ii) the CRLB falls within desired error thresholds.

Here, we provide an analytical expression for the second-order covariance term of MLEs obtained from general complex Gaussian data vectors, which can then be used in many practical problems since (i) data distributions can often be assumed to be Gaussian by virtue of the central limit theorem, and (ii) it allows for *both* the mean and the variance of the measurement to be functions of the estimation parameters, as is the case in the presence of signal-dependent noise. For example, the expression can be used to aid the design of many experiments in a variety of fields where nonlinear in-

[a)]Author to whom correspondence should be addressed. Electronic mail: makris@mit.edu

versions are typically performed and data are often corrupted by signal-dependent noise, such as ocean acoustics, geophysics, statistical signal processing and optics.[2–4]

We then consider the problem of source localization in a fluctuating ocean waveguide containing random internal waves and calculate the minimum array-gain-augmented signal to additive noise ratio (SANR) necessary for accurate localization. The fluctuating ocean waveguide is modeled using analytical expressions for the mean, spatial covariance, and mutual intensity[3] or the second spatial moment of the acoustic field forward propagated through random 3-D internal waves in a stratified ocean waveguide for a continuous wave (CW) narrowband signal.[5] This model provides an analytical treatment of the loss of inter-modal coherence in the forward propagating field due to scattering by internal waves. While the ensuing degradation in localization performance may be expected,[6,7] the exact effect of internal waves is here quantified for the first time by computing the asymptotic biases and variances of source localization estimates. The results presented here can be used to quantify the effects of environmental uncertainties on passive source localization techniques, such as matched-field processing (MFP) and focalization,[8] both of which typically utilize line arrays and CW signals.

Incomplete or imprecise knowledge of environmental parameters and randomness in the propagation environment are known to seriously deteriorate the performance of MFP, which has been investigated extensively in the past.[9–18] MFP has been demonstrated in a number of theoretical and experimental scenarios involving fluctuating or unknown environments,[14,17,18] but with significant localization ambiguities due to multimodal propagation and environmental mismatch. For example, in Ref. 18 it was shown that given 10 $\log_{10}$ SNR of more than 20 dB, peaks in the MFP ambiguity surface occurred at the true source range, but significant sidelobes were also observed at other ranges. All past experimental demonstrations of MFP have used SNRs that have exceeded the minimum levels necessary for accurate localization derived here.

Previously, the performance of passive source localization techniques was investigated by deriving CRLBs in a non-fluctuating waveguide.[6] Later it was shown that these were single-sample bounds,[19] multiple sample bounds were derived,[19,20] and it was shown that stationary averaging could reduce the bounds to zero.[19] Asymptotic statistics were then used to derive necessary conditions on sample size for errors to attain the CRLB and these were applied to source localization in a non-fluctuating waveguide.[21] Our approach is based on classical estimation theory,[1] is independent of the estimation technique and has already been applied in a variety of other problems, including time-delay and Doppler shift estimation,[1] pattern recognition in 2-D images,[22] geoacoustic parameter inversion,[23] and planetary terrain surface slope estimation.[24] In all previous applications except the last, however, the measurement was modeled as either (i) a deterministic signal vector, or (ii) a fully randomized signal vector with zero mean, both embedded in additive white noise. These are special cases of the scenario considered here where *both* the mean and the variance of the measurement are parameter-dependent, which is necessary to properly model acoustic propagation through a fluctuating waveguide that leads to a signal-dependent noise component. The methodology presented here can then be used in any experimental design to ensure that statistical biases and errors meet necessary error thresholds.

In Sec. II, we first review the first-order bias and first-order covariance of MLEs given general multivariate Gaussian data. We then provide a new analytic expression for the second-order covariance. In Sec. III, we calculate the MLE statistics and determine necessary conditions on sample size or SNR to obtain estimates that meet any design error threshold in a deterministic and a random waveguide.

II. GENERAL ASYMPTOTIC EXPANSIONS FOR THE BIAS AND COVARIANCE OF THE MLE

In this section, we first review the asymptotic expansions for the bias and covariance of the MLE. We also summarize the conditions necessary for an MLE to become asymptotically unbiased and have a variance that attains the CRLB. We then provide a new expression for the second-order covariance of the MLE given general multivariate Gaussian random data and describe how these measurements are obtained.

A. Asymptotic statistics of the MLE

Following the theory and notation adopted in Ref. 1, assume an experimental measurement that consists of a set of n independent and identically distributed N-dimensional real-valued random data vectors $\mathbf{X}_j$ obeying the conditional probability density $p(\mathbf{X};\boldsymbol{\theta})$, where $\mathbf{X}=[\mathbf{X}_1^T,\ldots,\mathbf{X}_n^T]$ and $\boldsymbol{\theta}$ is an m-dimensional parameter vector. The MLE $\hat{\boldsymbol{\theta}}$ of $\boldsymbol{\theta}$ is the maximum of the log-likelihood function $l(\boldsymbol{\theta})=\ln(p(\mathbf{X};\boldsymbol{\theta}))$ with respect to $\boldsymbol{\theta}$.[25–27] The first-order parameter derivative of the log-likelihood function is defined as $l_r=\partial l(\boldsymbol{\theta})/\partial\theta^r$, where θ^r is the rth component of $\boldsymbol{\theta}$. The elements of the expected information matrix, also known as the Fisher information matrix, are given by $i_{rs}=\langle l_r l_s\rangle$, and the elements of its inverse by $i^{rs}=[\mathbf{i}^{-1}]_{rs}$, where $\mathbf{i}^{-1}$ is the CRLB,[2,25,28] and $\langle\ldots\rangle$ signifies expected value. Moments of the log-likelihood derivatives are defined by $\upsilon_R\equiv\langle l_R\rangle$, and joint moments by $\upsilon_{R_1,R_2,\ldots,R_M}=\langle l_{R_1}l_{R_2}\ldots l_{R_M}\rangle$, where R_i is an arbitrary set of indices.[1,21]

The moments of $\hat{\theta}^r$ for $r=1,\ldots,m$ can then be expressed as a series of inverse powers of the sample size n,[1,21] provided that the required derivatives of the likelihood function exist.[29] The MLE bias is then given by[23,24]

$$\mathrm{bias}(\hat{\theta}^r,n)=b_1(\hat{\theta}^r;\boldsymbol{\theta},n)+b_2(\hat{\theta}^r;\boldsymbol{\theta},n)+\mathrm{Higher\ \ Order\ \ terms},\tag{1}$$

where $b_j(\hat{\theta}^r;\boldsymbol{\theta},n)=b_j(\hat{\theta}^r;\boldsymbol{\theta},1)/n^j$, so that

$$\mathrm{bias}(\hat{\theta}^r,n)=\frac{b_1(\hat{\theta}^r;\boldsymbol{\theta},1)}{n}+\frac{b_2(\hat{\theta}^r;\boldsymbol{\theta},1)}{n^2}+\mathrm{O}(n^{-3}),\tag{2}$$

where $\mathrm{O}(n^{-3})$ represents integer powers n^{-3} and higher. Similarly, the MLE variance can be written as

$$var(\hat{\theta}^r,n) = \frac{var_1(\hat{\theta}^r;\boldsymbol{\theta},1)}{n} + \frac{var_2(\hat{\theta}^r;\boldsymbol{\theta},1)}{n^2} + \mathrm{O}(n^{-3}), \quad (3)$$

where the first term on the right hand side of Eq. (3) is the CRLB, which is the asymptotic value of the variance when sample size n and SNR become large and also the minimum possible mean square error (MSE) of an unbiased estimate.

The value of n necessary for the MLE to become asymptotically unbiased is found by requiring the first-order bias to be much smaller than the true value of the parameter

$$n \gg \left| \frac{b_1(\hat{\theta}^r;\boldsymbol{\theta},1)}{\theta^r} \right|. \quad (4)$$

Similarly, the value of n necessary for the MLE variance to asymptotically attain the CRLB is found by requiring the second-order variance to be much smaller than the first-order, so that

$$n \gg \frac{|var_2(\hat{\theta}^r;\boldsymbol{\theta},1)|}{var_1(\hat{\theta}^r;\boldsymbol{\theta},1)}. \quad (5)$$

Only for values of n satisfying these conditions is it possible for the estimate to be in the asymptotic regime where it is unbiased and it continuously attains the CRLB,[1,21,23] so that it has the minimum possible mean square error. Following established convention,[21,23] we determine the sample sizes necessary to obtain an unbiased, minimum variance MLE by requiring the first-order bias and the second-order variance to be an order of magnitude smaller than the true value of the parameter and the first-order variance, respectively,

$$n_b \equiv 10 \left| \frac{b_1(\hat{\theta}^r;\boldsymbol{\theta},1)}{\theta^r} \right|, \quad (6a)$$

$$n_v \equiv 10 \frac{|var_2(\hat{\theta}^r;\boldsymbol{\theta},1)|}{var_1(\hat{\theta}^r;\boldsymbol{\theta},1)}. \quad (6b)$$

For the rest of this paper, conditions on sample size or SNR for parameter estimates to attain specified design error thresholds are calculated by requiring that (i) n meets the conditions in Eq. (6), and (ii) the CRLB is smaller than the desired error threshold. The sample size necessary to obtain accurate parameter estimates is then given by $(\max[n_b,n_v]) \times n'$, where

$$n' = \frac{\mathrm{CRLB}(\max[n_b,n_v])}{(\text{design threshold})^2}. \quad (7)$$

Expressions for $b_1(\hat{\theta}^r;\boldsymbol{\theta},n)$, $var_1(\hat{\theta}^r;\boldsymbol{\theta},n)$ and $var_2(\hat{\theta}^r;\boldsymbol{\theta},n)$ have been derived in terms of tensors in the form of $v_{R_1,R_2,\ldots,R_M}$ corresponding to moments of the log-likelihood derivatives,[1,30] as summarized below

$$b_1(\hat{\theta}^r;\boldsymbol{\theta},n) = \tfrac{1}{2} i^{ra} i^{bc} (v_{abc} + 2v_{ab,c}), \quad (8)$$

$$var_1(\hat{\theta}^r;\boldsymbol{\theta},n) = i^{rr}, \quad (9)$$

$$\begin{aligned} var_2(\hat{\theta}^r;\boldsymbol{\theta},n) &= -i^{rr} + i^{rm} i^{rm} \big[i^{pq} (2v_{mq,m,p} + v_{mmpq} + 3v_{mq,pm} \\ &\quad + 2v_{mmp,q} + v_{mpq,m}) + i^{pz} i^{qt} \big(v_{mpt} v_{m,q,z} + v_{mpm} v_{qzt} \\ &\quad + \tfrac{5}{2} v_{mpq} v_{mzt} + 2v_{m,qz} v_{mtp} + 2v_{mmt} v_{qz,p} + 6v_{mt,z} v_{mpq} \\ &\quad + v_{m,mt} v_{pqz} + 2v_{mq,z} v_{pt,m} + 2v_{mq,m} v_{pt,z} + v_{mq,p} v_{mt,z} \big) \big]. \end{aligned} \quad (10)$$

Here, as elsewhere, the Einstein summation convention is used, where summation over indices appearing both as superscript and subscript is implied. These expressions are evaluated for the case of multivariate Gaussian data next.

B. General multivariate Gaussian data

The general bias and variance expressions of Eqs. (8)–(10) are now applied to the specific case of data that obey the conditional Gaussian probability density[28]

$$\begin{aligned} p(\mathbf{X};\boldsymbol{\theta}) = \frac{1}{(2\pi)^{nN/2} |\mathbf{C}(\boldsymbol{\theta})|^{n/2}} \\ \times \exp\left\{ -\frac{1}{2} \sum_{j=1}^{n} (\mathbf{X}_j - \boldsymbol{\mu}(\boldsymbol{\theta}))^T \mathbf{C}(\boldsymbol{\theta})^{-1} (\mathbf{X}_j \right. \\ \left. - \boldsymbol{\mu}(\boldsymbol{\theta})) \right\}, \end{aligned} \quad (11)$$

where $\mathbf{C}$ is the real-valued covariance matrix, and $\boldsymbol{\mu}$ is the real-valued mean of the real random data. Similarly to the work of Ref. 21, in the present study of underwater localization, $\mathbf{X}_j$ represents the real and imaginary parts of the narrow-band acoustic data collected across an array of $N/2$ sensors around the given harmonic-source frequency, and the parameter set $\boldsymbol{\theta}$ represents the range and depth of the acoustic source.

The first-order bias has already been provided in Eq. (7) of Ref. 1 and is repeated below

$$\begin{aligned} b_1(\hat{\theta}^r;\boldsymbol{\theta},n) = -\tfrac{1}{2} i^{ra} i^{bc} \big(\boldsymbol{\mu}_{bc} \mathbf{C}^{-1} \boldsymbol{\mu}_a - \boldsymbol{\mu}_b (\mathbf{C}^{-1})_a \boldsymbol{\mu}_c \\ + \tfrac{1}{2} tr(\check{\mathbf{C}}_{bc} \check{\mathbf{C}}_a) \big). \end{aligned} \quad (12)$$

Typically, as discussed in the Introduction, both the data mean and covariance in Eq. (11) are functions of the desired parameter set $\boldsymbol{\theta}$. This necessitates evaluation of the joint moments in Eq. (10) as shown in Ref. 30 and summarized in Appendix B. The second-order covariance of the MLE given multivariate Gaussian random data is given by[30]

$$\begin{aligned} var_2(\hat{\theta}^r;\boldsymbol{\theta},n) = -i^{rr} + i^{rm} i^{rm} i^{ab} \big[\boldsymbol{\mu}_{ma} \mathbf{C}^{-1} \boldsymbol{\mu}_{mb} - \boldsymbol{\mu}_{mm} \mathbf{C}^{-1} \boldsymbol{\mu}_{ab} - \boldsymbol{\mu}_{mab} \mathbf{C}^{-1} \boldsymbol{\mu}_m + tr(\check{\mathbf{C}}_m \check{\mathbf{C}}_m \check{\mathbf{C}}_a \check{\mathbf{C}}_b) + tr(\check{\mathbf{C}}_m \check{\mathbf{C}}_a \check{\mathbf{C}}_m \check{\mathbf{C}}_b) \\ + tr(\check{\mathbf{C}}_{ab} \check{\mathbf{C}}_m \check{\mathbf{C}}_m) - tr(\check{\mathbf{C}}_{ma} \check{\mathbf{C}}_m \check{\mathbf{C}}_b) - tr(\check{\mathbf{C}}_{ma} \check{\mathbf{C}}_b \check{\mathbf{C}}_m) + \tfrac{1}{2} tr(\check{\mathbf{C}}_{ma} \check{\mathbf{C}}_{mb}) - \tfrac{1}{2} tr(\check{\mathbf{C}}_{mm} \check{\mathbf{C}}_{ab}) - \tfrac{1}{2} tr(\check{\mathbf{C}}_{mab} \check{\mathbf{C}}_m) \end{aligned}$$

$$+ 4\boldsymbol{\mu}_{ma}(\mathbf{C}^{-1})_m\boldsymbol{\mu}_b + 2\boldsymbol{\mu}_{ma}(\mathbf{C}^{-1})_b\boldsymbol{\mu}_m - \boldsymbol{\mu}_{ab}(\mathbf{C}^{-1})_m\boldsymbol{\mu}_m + \boldsymbol{\mu}_a(\mathbf{C}^{-1})_{mm}\boldsymbol{\mu}_b + \boldsymbol{\mu}_m(\mathbf{C}^{-1})_a(\mathbf{C}^{-1})_b\boldsymbol{\mu}_m$$
$$+ 2\boldsymbol{\mu}_m(\mathbf{C}^{-1})_a(\mathbf{C}^{-1})_m\boldsymbol{\mu}_b + \boldsymbol{\mu}_a(\mathbf{C}^{-1})_m(\mathbf{C}^{-1})_m\boldsymbol{\mu}_b\Big]$$
$$+ i^{rm}i^{rm}i^{ab}i^{cd}\Big\{\boldsymbol{\mu}_{ma}\mathbf{C}^{-1}\boldsymbol{\mu}_c[-\boldsymbol{\mu}_{md}\mathbf{C}^{-1}\boldsymbol{\mu}_b - 2\boldsymbol{\mu}_b(\mathbf{C}^{-1})_d\boldsymbol{\mu}_m - 4\boldsymbol{\mu}_b(\mathbf{C}^{-1})_m\boldsymbol{\mu}_d - tr(\check{\mathbf{C}}_{md}\check{\mathbf{C}}_b) + tr(\check{\mathbf{C}}_{bd}\check{\mathbf{C}}_m)$$
$$+ tr(\check{\mathbf{C}}_m\check{\mathbf{C}}_b\check{\mathbf{C}}_d) + tr(\check{\mathbf{C}}_m\check{\mathbf{C}}_d\check{\mathbf{C}}_b)] + \boldsymbol{\mu}_{ac}\mathbf{C}^{-1}\boldsymbol{\mu}_m\Big[\tfrac{1}{2}\boldsymbol{\mu}_{bd}\mathbf{C}^{-1}\boldsymbol{\mu}_m + 2\boldsymbol{\mu}_{mb}\mathbf{C}^{-1}\boldsymbol{\mu}_d + \tfrac{1}{2}tr(\check{\mathbf{C}}_{bd}\check{\mathbf{C}}_m) + tr(\check{\mathbf{C}}_{mb}\check{\mathbf{C}}_d)$$
$$- tr(\check{\mathbf{C}}_m\check{\mathbf{C}}_b\check{\mathbf{C}}_d)\Big] + tr(\check{\mathbf{C}}_m\check{\mathbf{C}}_a\check{\mathbf{C}}_c)\Big[\boldsymbol{\mu}_m(\mathbf{C}^{-1})_b\boldsymbol{\mu}_d + \boldsymbol{\mu}_m(\mathbf{C}^{-1})_d\boldsymbol{\mu}_b + 3\boldsymbol{\mu}_b(\mathbf{C}^{-1})_m\boldsymbol{\mu}_d + \tfrac{1}{2}(-tr(\check{\mathbf{C}}_m\check{\mathbf{C}}_b\check{\mathbf{C}}_d)$$
$$- tr(\check{\mathbf{C}}_m\check{\mathbf{C}}_d\check{\mathbf{C}}_b) + tr(\check{\mathbf{C}}_{md}\check{\mathbf{C}}_b) + tr(\check{\mathbf{C}}_{mb}\check{\mathbf{C}}_d) - tr(\check{\mathbf{C}}_{bd}\check{\mathbf{C}}_m))\Big] + tr(\check{\mathbf{C}}_{ma}\check{\mathbf{C}}_c)\Big[-\tfrac{1}{4}tr(\check{\mathbf{C}}_{md}\check{\mathbf{C}}_b) - \boldsymbol{\mu}_m(\mathbf{C}^{-1})_d\boldsymbol{\mu}_b$$
$$- 2\boldsymbol{\mu}_b(\mathbf{C}^{-1})_m\boldsymbol{\mu}_d\Big] - \tfrac{3}{2}\boldsymbol{\mu}_a(\mathbf{C}^{-1})_m\boldsymbol{\mu}_c\boldsymbol{\mu}_b(\mathbf{C}^{-1})_m\boldsymbol{\mu}_d + tr(\check{\mathbf{C}}_{ac}\check{\mathbf{C}}_m)\Big[\tfrac{1}{2}tr(\check{\mathbf{C}}_{mb}\check{\mathbf{C}}_d) + \tfrac{1}{8}tr(\check{\mathbf{C}}_{bd}\check{\mathbf{C}}_m)\Big] + \boldsymbol{\mu}_m(\mathbf{C}^{-1})_a\boldsymbol{\mu}_c[$$
$$- \boldsymbol{\mu}_m(\mathbf{C}^{-1})_d\boldsymbol{\mu}_b - 2\boldsymbol{\mu}_b(\mathbf{C}^{-1})_m\boldsymbol{\mu}_d] + \Big[\boldsymbol{\mu}_{cd}\mathbf{C}^{-1}\boldsymbol{\mu}_a - \boldsymbol{\mu}_c(\mathbf{C}^{-1})_a\boldsymbol{\mu}_d + \tfrac{1}{2}tr(\check{\mathbf{C}}_{cd}\check{\mathbf{C}}_a)\Big]\Big[\tfrac{1}{2}tr(\check{\mathbf{C}}_{mm}\check{\mathbf{C}}_b) + \tfrac{1}{2}tr(\check{\mathbf{C}}_{mb}\check{\mathbf{C}}_m)$$
$$- tr(\check{\mathbf{C}}_m\check{\mathbf{C}}_m\check{\mathbf{C}}_b) + \boldsymbol{\mu}_{mm}\mathbf{C}^{-1}\boldsymbol{\mu}_b + \boldsymbol{\mu}_{mb}\mathbf{C}^{-1}\boldsymbol{\mu}_m + \boldsymbol{\mu}_m(\mathbf{C}^{-1})_m\boldsymbol{\mu}_b\Big]\Big\}, \tag{13}$$

where subscripts indicate derivatives with respect to the specified indices, $tr(\mathbf{C})$ stands for the trace of $\mathbf{C}$, and the auxiliary term $\check{\mathbf{C}}_R$ is defined in Eq. (B1c) for an arbitrary set of indices R. As shown in Appendix B, the above expression can be used even if the random data are not distributed in a Gaussian form, provided that they can be expressed as functions of Gaussian random variables with a Jacobian of the transformation that is independent of the parameter set $\boldsymbol{\theta}$.[30] Eq. (13) can be used to calculate the second-order MLE covariance in applications where *both* the data mean and covariance are functions of the estimated parameters.

C. Mean and variance of the measured field

We consider a vertical receiving array employed to localize a harmonic source in a fluctuating ocean waveguide. The mean and covariance of the measured field can then be obtained from the analytical expressions provided in Ref. 5 and summarized in Appendix A. Equation (A1) defines the qth element of the vector $\bar{\boldsymbol{\mu}}$ for $q=1,2,3,\ldots,N/2$, where $N/2$ is the number of hydrophones in the receiving array. Similarly, Eq. (A4) defines the (q,p) element of the covariance matrix $\bar{\mathbf{C}}$ for $q,p=1,2,3,\ldots,N/2$. In the above, we have defined the complex mean $\bar{\boldsymbol{\mu}}$ and covariance $\bar{\mathbf{C}}$ that are related to the real mean $\boldsymbol{\mu}$ and covariance $\mathbf{C}$ of Eq. (11) by the following expressions:[28]

$$\boldsymbol{\mu} = \begin{bmatrix} \mathrm{Re}(\bar{\boldsymbol{\mu}}) \\ \mathrm{Im}(\bar{\boldsymbol{\mu}}) \end{bmatrix}, \quad \mathbf{C} = \frac{1}{2}\begin{bmatrix} \mathrm{Re}(\bar{\mathbf{C}}) & -\mathrm{Im}(\bar{\mathbf{C}}) \\ \mathrm{Im}(\bar{\mathbf{C}}) & \mathrm{Re}(\bar{\mathbf{C}}) \end{bmatrix} + \sigma_{an}^2\mathbf{I}, \tag{14}$$

where $\mathbf{I}$ is the identity matrix and σ_{an}^2 is defined as the instantaneous variance of the additive noise on each hydrophone. The expressions above are valid under the assumption that the complex Fourier transform of the data measured at each hydrophone follow a circularly complex Gaussian random process[3,31] when the mean is subtracted. Evaluation of Eqs. (8)–(10) requires knowledge of the higher-order derivatives of $\boldsymbol{\mu}$ and $\mathbf{C}$ with respect to parameters ρ and z_0, which are provided in Appendix A.

The SNR and signal to additive noise ratio (SANR) for a single sample collected across the array are then defined as

$$\mathrm{SNR}[1] = \frac{\sum_{q=1}^{N/2}|\langle\Psi_T(\mathbf{r}_q|\mathbf{r}_0)\rangle|^2}{\sum_{q=1}^{N/2}[Var(\Psi_T(\mathbf{r}_q|\mathbf{r}_0)) + \sigma_{an}^2]} = \frac{tr(|\bar{\boldsymbol{\mu}}|^2)}{tr(\bar{\mathbf{C}}) + N\sigma_{an}^2/2}, \tag{15}$$

$$\mathrm{SANR}[1] = \frac{\sum_{q=1}^{N/2}[|\langle\Psi_T(\mathbf{r}_q|\mathbf{r}_0)\rangle|^2 + Var(\Psi_T(\mathbf{r}_q|\mathbf{r}_0))]}{N\sigma_{an}^2/2} = \frac{tr(|\bar{\boldsymbol{\mu}}|^2) + tr(\bar{\mathbf{C}})}{N\sigma_{an}^2/2}, \tag{16}$$

where $\mathbf{r}_q$ is the position of the qth hydrophone on the receiver array, and $\mathbf{r_0}$ is the position of the source. Since the total received intensity is given by the numerator of Eq. (16), we adopt the convention[21] of setting the SNR[1] of the field across the array to unity *for a source located at r = 1 km range and any depth z*, to maintain consistency between the different waveguides examined in the next section. The definition provided in Eq. (16) does not account for potential improvements due to array gain. For a uniform array of $N/2$ elements, the SANR[1] can be array-gain-augmented by $(N/2)$ for the ideal case of a plane wave signal embedded in spatially uncorrelated white noise.[2] For a deterministic signal embedded in additive white noise, the covariance matrix $\mathbf{C}$ reduces to $\sigma_{an}^2\mathbf{I}$ so that SNR and SANR are equal and proportional to sample size,[21]

$$n = \frac{\mathrm{SANR}}{\mathrm{SANR}[1]}. \tag{17}$$

The sample size conditions in Eqs. (6) and (7) can then also be written in terms of SANR and SANR[1]. For general multivariate Gaussian data, this simple proportionality is

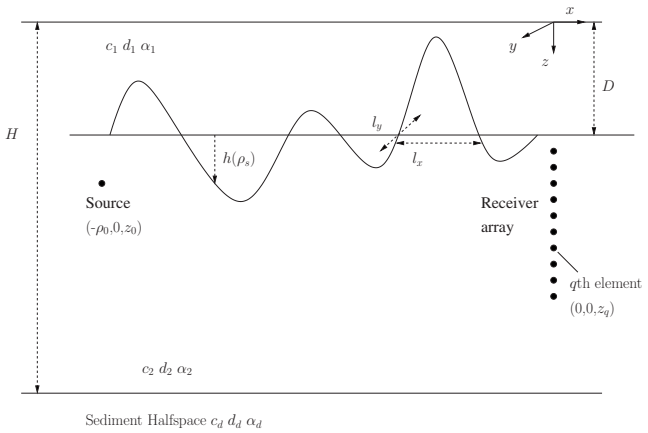

FIG. 1. Geometry of an ocean waveguide environment with two-layer water column of total depth $H=100$ m, and upper layer depth of $D=30$ m. The density and sound speed in the upper layer are $d_1=1024$ kg/m^3 and $c_1=1520$ m/s, respectively. The density and sound speed in the lower layer are $d_2=1025$ kg/m^3 and $c_2=1500$ m/s, respectively. The bottom sediment half-space is composed of sand with density $d_b=1.9$ g/cm^3 and sound speed $c_b=1900$ m/s. The attenuations in the water column and bottom are $\alpha_1=\alpha_2=6\times10^{-5}$ dB/λ and $\alpha_b=0.8$ dB/λ, respectively. The internal wave disturbances have coherence length scales $l_x=100$ m and $l_y=100$ m in the x and y directions, respectively, and are measured with positive height h measured downward from the interface between the upper and lower water layers. The internal wave disturbances, when present, are assumed to have a height standard deviation of $\eta_h=4$ m. In the case of a deterministic waveguide with no internal waves, $h=0$ m.

only approximately valid when the signal-dependent noise contribution to the covariance is weak.

III. ILLUSTRATIVE EXAMPLES

Here we demonstrate how the methodology presented in Sec. II A and the expression for the MLE second-order covariance in Eq. (13) can be used to specify conditions on sample size or SNR to obtain accurate source localization estimates in a fluctuating ocean waveguide. The effects of the loss of coherence in the forward propagating field are quantified by (i) calculating these sample sizes and SNRs, as well as the asymptotic biases and variances of source localization MLEs, and (ii) comparing them to those for a static waveguide. In the latter, the measured acoustic field is fully coherent, and the source localization problem reduces to that of parameter estimation given a deterministic signal embedded in white additive Gaussian noise. Such a problem was treated for a different waveguide, source frequency and receiving array in Ref. 21, and results are presented here for comparison with the fluctuating waveguide case considered. In the fluctuating waveguide, both the mean and the variance of the measurement are parameter dependent so that Eq. (13) must be used to correctly calculate the asymptotic MLE variance. The internal wave height standard deviation is chosen to be greater than the acoustic wavelength so that the waveguide becomes highly randomized within a few kilometers of the source,[5] and the effects of environmental uncertainty on source localization can be distinguished.

The simple two-layer waveguide used in Ref. 5 is again employed here to model internal waves in a shallow-water continental shelf environment. Figure 1 shows the selected sound speed profile, bottom composition and internal wave characteristics. The origin of the coordinate system is placed at the sea surface. The z axis points downward and normal to the interface between horizontal strata. The water depth is H and the boundary separating the upper and lower medium is at depth $z=D$. Let coordinates of the source be defined by $\mathbf{r_0}=(-\rho_0,0,z_0)$, and receiver coordinates by $\mathbf{r}=(0,0,z)$. Spatial cylindrical (ρ,ϕ,z) and spherical systems (r,θ,ϕ) are defined by $x=r\sin\theta\cos\phi$, $y=r\sin\theta\sin\phi$, $z=r\cos\theta$, and $\rho=\sqrt{x^2+y^2}$. The horizontal and vertical wave number components for the nth mode are, respectively, $\xi_n=k\sin\alpha_n$ and $\gamma_n=k\cos\alpha_n$, where α_n is the elevation angle of the mode measured from the z axis. Here, $0\le\alpha_n\le\pi/2$ so that down- and up-going plane wave components of each mode will then have elevation angles α_n and $\pi-\alpha_n$, respectively. The azimuth angle of the modal plane wave is denoted by β, where $0\le\beta\le2\pi$. The geometry of spatial and wave number coordinates is shown in Ref. 32.

For single frequency simulations, we employ a 415 Hz monopole source and a 10-element vertical array in a 100 m deep waveguide. The water column is comprised of a warm upper layer with density $d_1=1024$ kg/m^3 and sound speed $c_1=1520$ m/s overlying a cool lower layer with density $d_2=1025$ kg/m^3 and sound speed $c_2=1500$ m/s. The boundary between the layers is at a depth of $D=30$ m, and the attenuation in both layers is $\alpha=6\times10^{-5}$ dB/λ. The spacing of the array elements is 1.5 m ($\lambda/2\approx1.8$ m) with the shallowest element at 43.5 m, so that the array is centered in the water column. The ocean bottom is a fluid half space with a sound speed of $c_b=1700$ m/s, a density of $d_b=1.9$ kg/m^3, and an attenuation of $\alpha_b=0.8$ dB/wavelength, which are representative values for sandy environments.

Note that the results presented in this paper are not representative of the performance of the waveguide invariant[33,34] or the array invariant,[35] since the former uses acoustic intensity data versus range and frequency and the latter employs beam-time or coherent hydrophone data over time. Here, we instead consider instantaneous measurements of the acoustic field due to a CW source made with a vertical line array. The results presented here can also be used for broadband signals when matched-field processing is performed separately for each frequency component and the computed ambiguity surfaces are then combined incoherently. This is commonly known as incoherent processing,[18,36] even though each separate frequency bin is still processed coherently before the correlation values of the data and replica fields are averaged. For a broadband signal that consists of M_f frequency bins, incoherent averaging means that the effective sample size equals $n\times M_f$, so that conditions on the necessary sample sizes can be found by scaling the right hand sides of Eqs. (6a), (6b), and (7) by $1/M_f$.

A. Undisturbed waveguide

For the undisturbed static waveguide, coherent interference between the waveguide modes leads to a range- and depth-dependent structure in the total acoustic field intensity which maintains a modal coherence pattern over very long ranges with the SANR range-depth pattern of Fig. 2. The

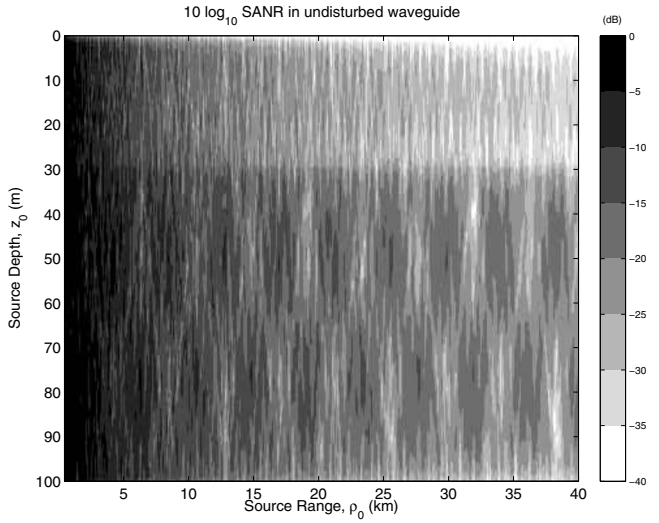

FIG. 2. Signal to additive noise ratio (SANR) at 415 Hz in an undisturbed waveguide with no internal waves. The SANR received at the 10-element vertical array described in Sec. III is plotted as a function of source range ρ_0 and depth z_0. The observed range-depth pattern is due to the underlying modal coherence structure of the total acoustic field intensity. The receiver array is centered at $\rho=0$ m and $z=50$ m. The source level is fixed as a constant over range so that 10 $\log_{10}$ SANR[1] is 0 dB at 1 km source range at all source depths. For the undisturbed waveguide, SANR is equivalent to signal to noise ratio (SNR).

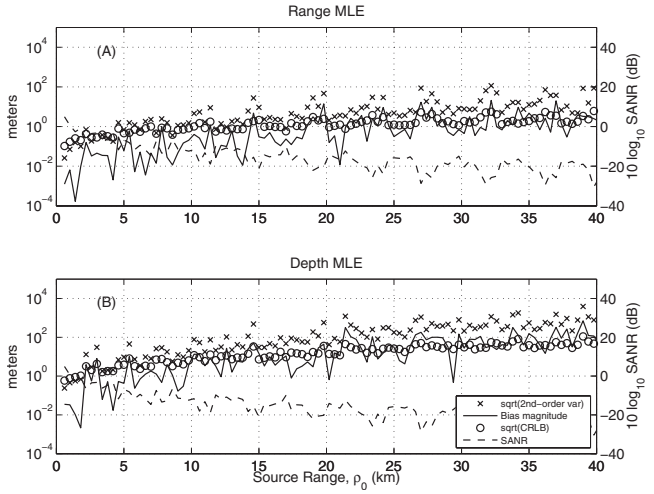

FIG. 3. Ocean acoustic localization MLE behavior given a single sample for (a) range estimation and (b) depth estimation for a 415 Hz source placed at 50 m depth in an undisturbed waveguide with no internal waves. The MLE first-order bias magnitude (solid line), square root of the CRLB (circle marks) and square root of the second-order variance (cross marks), as well as the measured signal to additive noise ratio (SANR, dashed line) are plotted as functions of source range. Given the necessary sample size conditions in Eq. (6), whenever the first-order bias and the second-order variance attain roughly 10% of the true parameter value and the CRLB, respectively, more than a single sample will be needed to obtain unbiased, minimum variance MLEs. The source level is fixed as a constant over range so that 10 $\log_{10}$ SANR[1] is 0 dB at 1 km source range.

SANR[1] is computed using Eq. (16) and plotted as a function of source-receiver range and source depth for the shallow water waveguide of Fig. 1 when there are no internal waves present. The source level is fixed as a constant over range so that 10 $\log_{10}$ SANR[1] is 0 dB across the array for a source-receiver range of 1 km. For the static waveguide, the covariance of the acoustic field measurement in Eq. (14) reduces to $\mathbf{C}=\sigma_{an}^2\mathbf{I}$ so that SNR[1] and SANR[1] in Eqs. (15) and (16) are equivalent. For the array of 10 elements considered here, the array-gain-augmented SANR[1] is higher than the SANR[1] shown in Fig. 2 by a factor of 10.

The first-order bias, first-order covariance (CRLB) and second-order covariance of the MLEs for source range and depth are plotted in Fig. 3, given a source fixed at 50 m depth and a sample size of $n=1$. The asymptotic bias and the square root of the CRLB for a range estimate are very small, typically less than 10 m even at ranges beyond 30–40 km, while the corresponding quantities for a depth estimate [Fig. 3(b)] reach values comparable to the waveguide depth of 100 m. This suggests that it may be possible to obtain unbiased range MLEs from a single sample, whereas depth MLEs will have significant biases, *given the SANR[1] in Fig. 2*. The second-order covariance exceeds the CRLB for both the range and depth MLE even at a few kilometers from the source, so that the variance of MLEs obtained from a single sample will not in general attain the CRLB. The CRLB and the second-order covariance approximately coincide where 10 $\log_{10}$ SANR[1] is about -5 dB, which is where the array-gain-augmented 10 $\log_{10}$ SANR[1] equals 5 dB. Increasing the array gain could help obtain single-sample MLEs that attain the CRLB at longer ranges from the source.

The results shown here are consistent with those of Figs. 2 and 4 of Ref. 21 for a deterministic source signal in a static waveguide, as expected. Since the bias and variance terms in the asymptotic expansions of the MLE moments, e.g. Equation (3), always depend on inverse order of sample size n, the asymptotic statistics of the MLE for any arbitrary n can be obtained by shifting the curves in Fig. 3 according to the order of the term involved and the value of n desired for a given SANR[1]. For the static waveguide, the data covariance $\mathbf{C}$ is parameter independent, in which case the MLE bias and covariance can also be expanded in inverse orders of SNR.[30] The necessary sample sizes given throughout this section can then also be interpreted in terms of necessary SNR or SANR. Increasing SANR by a factor of 10 in Fig. 3, for example, would reduce the first-order bias and the CRLB by one order of magnitude, and the second-order covariance by two orders of magnitude, as seen by replacing n in Eqs. (2) and (3) with SANR/SANR[1] [Eq. (17)]. Minimum variance range MLEs could then be obtained from a single sample up to the maximum range for which the second-order covariance and the CRLB are equal in Fig. 3, i.e., 8 km, given such a factor of 10 increase in SANR.

Figure 4 shows the sample size n necessary to obtain an unbiased source range MLE whose mean square error (MSE) attains the CRLB and has $\sqrt{\text{CRLB}}\leq 100$ m. It also shows that for fixed SANR, n fluctuates as a function of source range due to the modal interference structure of the static waveguide. If the received 10 $\log_{10}$ SANR is fixed at 0 dB for all ranges between 1 and 50 km, then to obtain a source range estimate of 100 m accuracy for 95% of the ranges either (a) 20 samples are needed, or (b) given a single sample a 10 $\log_{10}$ SANR of 13 dB [Eq. (17)] is necessary.

Figures 5(a) and 5(b) show the square root of the single-sample CRLB for source range and depth estimation. The

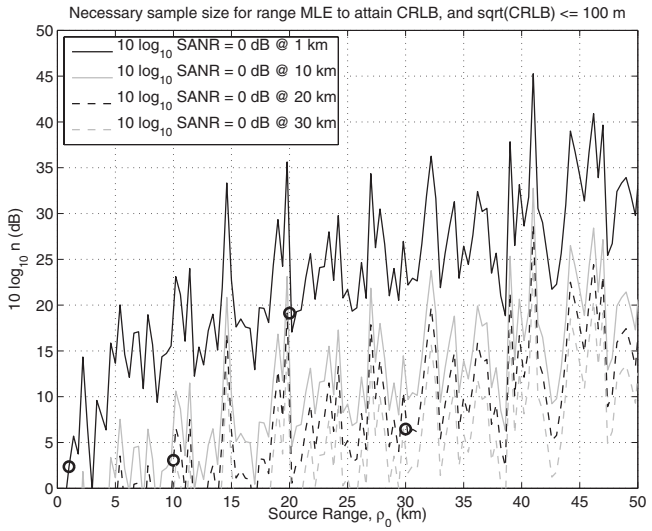

FIG. 4. Undisturbed waveguide. $10\log_{10} n$, where $n=\{\max[n_b,n_v]\times n'\}$ is the sample size necessary to obtain an unbiased source range MLE whose MSE attains the CRLB and has $\sqrt{\text{CRLB}}\leq 100$ m, where n_b, n_v, n' are calculated using Eqs. (6) and (7), given a 415 Hz source at 50 m depth. Source level is fixed as a constant over range so that $10\log_{10}$ SANR is 0 dB at 1, 10, 20, and 30 km source range (black circles), respectively, for the four curves shown.

sample sizes necessary to obtain unbiased source range and depth estimates that asymptotically attain the CRLB are given by the maximum of n_b, n_v in Eq. (6) and shown in Figs. 5(c) and 5(d). They are found to be roughly inversely proportional to SANR[1] and are typically much larger than one, as expected from Fig. 3. We find that the necessary sample size is at least an order of magnitude larger in the upper waveguide layer where SANR[1] decreases more rapidly, as can be seen in Fig. 2. Given sufficient source level,

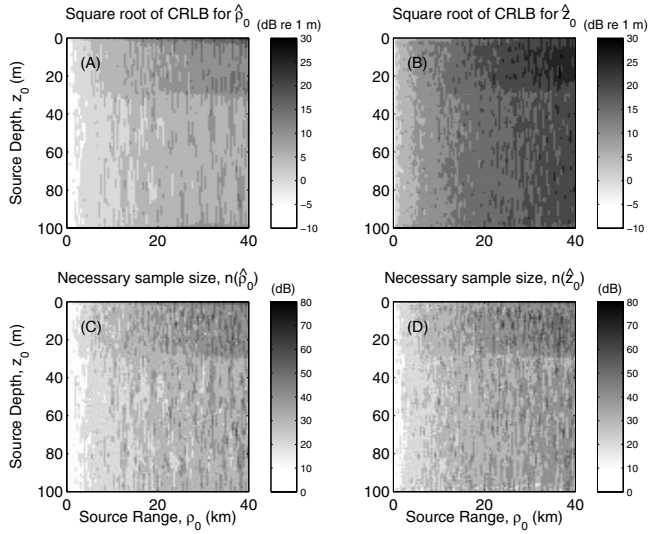

FIG. 5. Undisturbed waveguide. $10\log_{10}$ of the square root of the CRLB for (a) source range $\hat{\rho}_0$, (b) source depth $\hat{z}_0$ MLEs given a single sample. $10\log_{10}(\max[n_b,n_v])$, the sample sizes or SNRs necessary to obtain (c) source range, (d) source depth MLEs that become unbiased and have MSEs that attain the CRLB. Given any design error threshold, the sample size necessary to obtain an accurate source range or depth MLE is then equal to $(\max[n_b,n_v])\times n'$, where $n'=\text{CRLB}(\max[n_b,n_v])/(\text{design threshold})^2$. The source level is fixed as a constant over range so that $10\log_{10}$ SANR[1] is 0 dB at 1 km source range at all source depths.

however, accurate range MLEs may be obtained from a single sample at any desired source-receiver separation. For example, increasing source level so that $10\log_{10}$ SANR at 1 km range is 40 dB should be sufficient to accurately estimate the range of a source at any depth and ranges up to roughly 30 km, according to Fig. 5 and Eq. (17).

Given the sample sizes in Fig. 5(c), for example, the source range MLE will be in the asymptotic regime where its variance continuously attains the CRLB, which is the minimum possible MSE of an unbiased estimate, regardless of the method of estimation. Since the CRLB is inversely proportional to sample size, as shown in Eq. (3), conditions can be specified on sample size for the MLE error to meet any desired threshold. It is then possible to determine whether these conditions can be met in practice, since the number of statistically independent samples of the received acoustic signal is limited by the ratio of the measurement time window to the coherence time scale of acoustic field intensity,[1,31] which can also be calculated.[37]

The temporal coherence scale of acoustic field fluctuations for a shallow-water continental shelf environment such as the one considered here is on the order of minutes,[37] so that the calculated necessary sample sizes imply that accurate source localization may not be practical at ranges greater than 20 km *given the SANR[1] in Fig. 2*, since stationary averaging over time periods on the order of hours may then be necessary.

B. Waveguide containing internal waves

The fluctuating waveguide considered here is the same as that in Ref. 5, where the geometry, variables and parameters of the waveguide are also provided here in Fig. 1. The variance of the acoustic field intensity, or incoherent intensity, starts dominating the expected total intensity for ranges beyond roughly a few kilometers in the upper layer and 20 km in the lower waveguide layer, as seen in Fig. 6(c). The SNR[1] and SANR[1] are computed using Eqs. (15) and (16), respectively, and are plotted together with the ratio of coherent to incoherent intensity in Figs. 6(a)–6(c) as functions of source-receiver range and source depth for a waveguide containing random internal waves. The forward propagated field quickly loses its modal coherence structure and follows a decaying trend with local oscillations over range due to scattering by random 3-D internal waves. The internal wave disturbances have a height standard deviation of $\eta_h=4$ m and coherence lengths of $l_x=l_y=100$ m.[5] In this random waveguide, there is no longer a simple linear relationship between SNR[1] and SANR[1], but $10\log_{10}$ SNR[1] can be approximated as equal to $10\log_{10}$ SANR[1] minus 4–5 dB for ranges beyond roughly 30 km, as can be seen by comparing Figs. 6(a) and 6(b), as well as in Fig. 7.

The loss of coherence in the forward propagated field has severe effects on localization accuracy, as shown in Fig. 7 where the first-order bias, first-order covariance (CRLB) and second-order covariance of source position MLEs are plotted given a source fixed at 50 m depth and a sample size of $n=1$. While the asymptotic bias and square root of the CRLB of the source range estimate [Fig. 7(a)] are still found

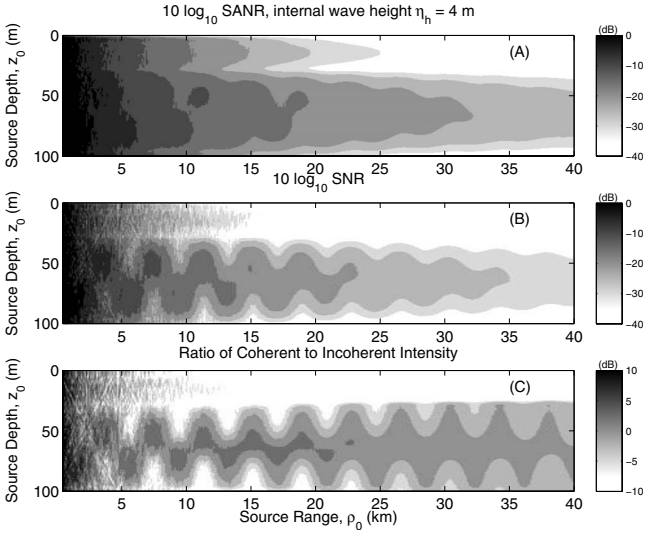

FIG. 6. (a) Signal to additive noise ratio (SANR), (b) signal to noise ratio (SNR), and (c) the ratio of coherent to incoherent intensity at 415 Hz in a waveguide containing random internal waves. The internal wave disturbances have a height standard deviation of $\eta_h=4$ m and coherence lengths of $l_x=l_y=100$ m. This medium is highly random so that incoherent intensity dominates at all depths beyond about 20 km. The total received intensity, given by the numerator of SANR in Eq. (16) follows a decaying trend with local oscillations over range. All quantities are plotted as functions of source range ρ_0 and depth z_0 received at the 10-element vertical array described in Sec. III. The receiver array is centered at $\rho=0$ m and $z=50$ m. The source level is fixed as a constant over range so that 10 $\log_{10}$ SANR[1] is 0 dB at 1 km source range at all source depths

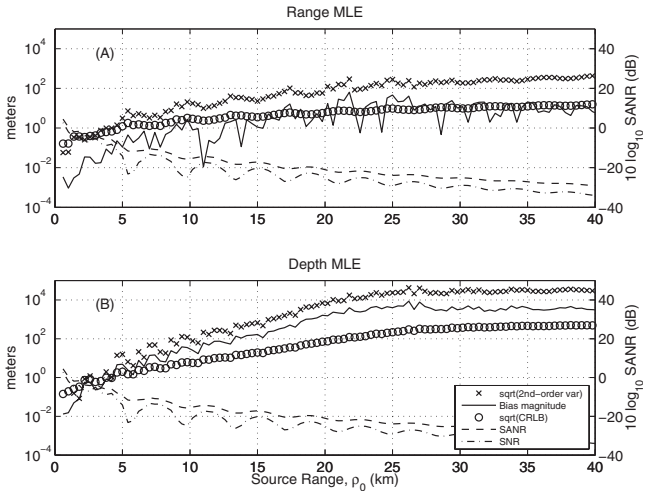

FIG. 7. Ocean acoustic localization MLE behavior given a single sample for (a) range estimation and (b) depth estimation for a 415 Hz source placed at 50 m depth in a waveguide containing random internal waves. The internal wave disturbances have a height standard deviation of $\eta_h=4$ m and coherence lengths of $l_x=l_y=100$ m. The MLE first-order bias magnitude (solid line), square root of the CRLB (circle marks) and square root of the second-order variance (cross marks), as well as the signal to additive noise ratio (SANR, dashed line) and signal to noise ratio (SNR, dash-dotted line) are plotted as functions of source range. Other than the first-order bias and CRLB of the range MLE, the remaining quantities have increased by at least an order of magnitude when compared to the static waveguide scenario in Fig. 3. Given the necessary sample size conditions in Eq. (6), whenever the first-order bias and the second-order variance attain roughly 10% of the true parameter value and the CRLB, respectively, more than a single sample will be needed to obtain unbiased, minimum variance MLEs. The source level is fixed as a constant over range so that 10 $\log_{10}$ SANR[1] is 0 dB at 1 km source range.

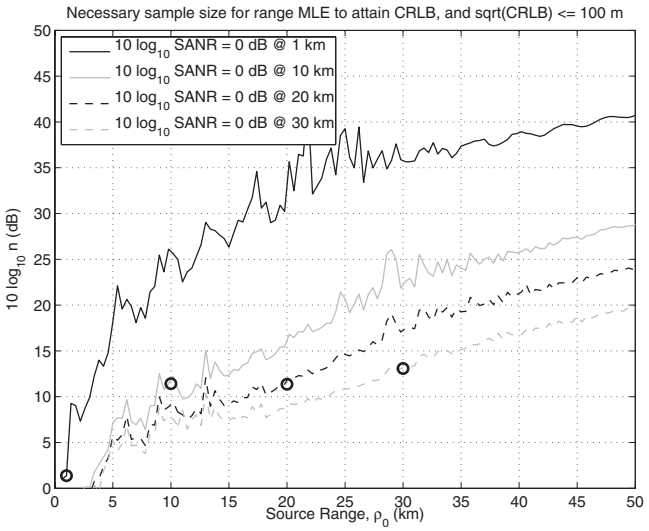

FIG. 8. Fluctuating waveguide containing internal waves. 10 $\log_{10} n$, where $n=\{\max[n_b,n_v]\times n'\}$ is the sample size necessary to obtain an unbiased source range MLE whose MSE attains the CRLB and has $\sqrt{\text{CRLB}} \leq 100$ m, and n_b, n_v, n' are calculated using Eqs. (6) and (7), given a 415 Hz source placed at 50 m depth. Source level is fixed as a constant over range so that 10 $\log_{10}$ SANR is 0 dB at 1, 10, 20, and 30 km source range (black circles), respectively, for the four curves shown.

to be relatively small, on the order of 10 m for source-receiver ranges greater than about 20 km, the square root of the second-order range variance has increased by approximately an order of magnitude from the static waveguide case. The asymptotic bias and variances of the source depth MLE have all increased by an order of magnitude or more, as seen by comparing Figs. 7(b) and 3(b). Similarly to the undisturbed waveguide scenario, increasing the array gain could help improve the accuracy of source localization MLEs.

Given Eq. (6b), significantly larger sample sizes will be necessary to obtain unbiased range MLEs that attain the minimum possible mean square error compared to the static waveguide case. It will also be practically impossible to attain an accurate source depth estimate from a single sample for ranges greater than a couple of kilometers, given the SANR[1] in Fig. 6. For a given SANR[1], the asymptotic statistics of the MLE for any arbitrary n can be obtained by shifting the curves in Fig. 7 according to the order of the term involved and the value of n desired. For this random waveguide, the data covariance $\mathbf{C}$ is parameter dependent and the MLE bias and covariance cannot be readily expanded in inverse orders of SANR.[30] We find that increasing SANR by a factor of 10 in Fig. 7 reduces the first-order bias and the CRLB by roughly one order of magnitude, and the second-order covariance by approximately two orders of magnitude, as in the deterministic waveguide case. Minimum variance range MLEs can then be obtained from a single sample up to the maximum range for which the second-order covariance and the CRLB are equal in Fig. 7, i.e. 5 km, given such a factor of 10 increase in SANR.

Figure 8 shows the sample size n necessary to obtain an unbiased source range MLE whose MSE attains the CRLB and has $\sqrt{\text{CRLB}} \leq 100$ m. It also shows that for fixed SANR, n remains approximately constant as function of

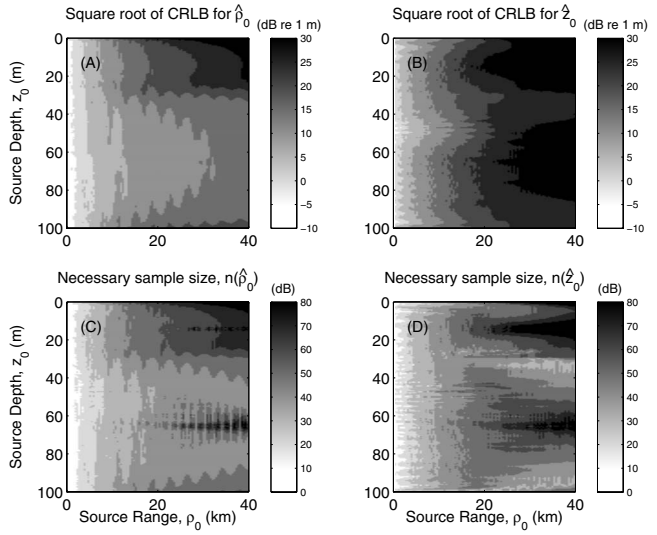

FIG. 9. Fluctuating waveguide containing internal waves. $10\log_{10}$ of the square root of the CRLB for (a) source range $\hat{\rho}_0$, (b) source depth $\hat{z}_0$ MLEs given a single sample. $10\log_{10}(\max[n_b,n_v])$, the sample sizes or SNRs necessary to obtain (c) source range, (d) source depth MLEs that become unbiased and have MSEs that attain the CRLB. Given any design error threshold, the sample size necessary to obtain an accurate source range or depth MLE is then equal to $(\max[n_b,n_v])\times n'$, where $n'=\mathrm{CRLB}(\max[n_b,n_v])/(\text{design threshold})^2$. The internal wave disturbances have a height standard deviation of $\eta_b=4$ m and coherence lengths of $l_x=l_y=100$ m. The source level is fixed as a constant over range so that $10\log_{10}$ SANR[1] is 0 dB at 1 km source range at all source depths.

source range in the fluctuating waveguide, since the forward propagated field now follows a smoother trend with range than the undisturbed waveguide due to scattering by random 3-D internal waves. If the received $10\log_{10}$ SANR is fixed at 0 dB for the four source ranges investigated in Fig. 8 (1, 10, 20, and 30 km), then to obtain a source range estimate of 100 m accuracy either (a) 20 samples are needed, or (b) given a single sample a $10\log_{10}$ SANR of 13 dB [Eq. (17)] is necessary.

The presence of internal waves may severely affect the ability to obtain accurate estimates of source position in practice, as can be deduced from Figs. 9(a) and 9(b) which show the square root of the single-sample CRLB for source range and depth estimation. The sample sizes necessary to obtain unbiased source range and depth estimates which asymptotically attain the CRLB are shown in Figs. 9(c) and 9(d) and are typically much larger than one, as expected from Fig. 7.

The minimum error of an unbiased source range MLE is on the order of tens of meters even at ranges beyond 20 km for a source in the lower waveguide layer, as expected from Fig. 7(a), but may become as high as several hundred meters for a source in the upper layer where the SANR[1] is much lower, as seen in Fig. 6. The minimum error of an unbiased source depth MLE has increased from the undisturbed waveguide case by at least an order of magnitude, as expected from Fig. 7(b). The sample sizes necessary to attain either of these CRLBs have also increased by an order of magnitude or more from those corresponding to the static waveguide scenario, Fig. 5. These increases in the CRLBs and the necessary sample sizes to attain them are particularly pronounced in the upper layer of the waveguide and the middle of the lower layer at about 65 m, since those are the regions of most rapid SNR[1] and SANR[1] decrease, and also where the received intensity is weakly dependent on source depth and range.

The calculated necessary sample sizes suggest that it becomes practically impossible to accurately estimate source position for ranges greater than a few kilometers for the specific receiver array, waveguide, source frequency and type of instantaneous measurements considered *given the SANR[1] in Fig. 6(a)* and typical acoustic field coherent scales,[5] since stationary averaging over tens of hours may be required. The examples presented here illustrate passive source localization scenarios typical of matched-field processing (MFP) and focalization[8] in fluctuating waveguides.[5,38–40] They not only provide a quantitative demonstration of the degradation in localization accuracy due to the presence of internal waves, but can also be used to assess the effects of environmental uncertainties on parameter estimation.

1. Importance of the joint-moment terms in calculating the second-order covariance

Here, we show the benefits of employing the expression for the MLE second-order covariance in Eq. (13) that can be used to determine necessary sample size conditions for accurate estimation given measurements whose mean and covariance are *both* parameter dependent. If the physical environment leads to parameter dependence in both the mean and covariance and this dependence is neglected in either, then large errors can easily ensue, as demonstrated for the physical scenario considered in Sec. III B. Neglecting the parameter dependence in either the covariance or the mean is equivalent to approximating the underwater acoustic measurement as either (i) a deterministic signal vector, or (ii) a fully randomized signal vector with zero mean, both embedded in additive white noise.

These two common approximations to the received field may lead to significant miscalculations of the CRLB and the necessary sample sizes of Eq. (6), as can be seen by comparing Figs. 7 and 9 to Figs. 10 and 11 and Figs. 12 and 13, respectively. Note that the asymptotic biases and variances for source range and depth MLEs [Figs. 10(a) and 10(b), respectively] are of the same order of magnitude as those for the undisturbed waveguide in Fig. 3. This is expected since neglecting parameter dependence in the covariance $\mathbf{C}$ is equivalent to assuming a static waveguide where the only noise is purely white additive. The asymptotic biases and variances for the case where $\boldsymbol{\mu}$ is assumed parameter independent [Figs. 11(a) and 11(b)] are instead found to be many orders of magnitude larger. The observed increase is much larger than the decrease in SANR[1] and SNR[1], and suggests that the covariance of the measurement is only weakly dependent on source range and depth. The differences observed between Figs. 10 and 11 are consistent with those observed between Figs. 2 and 3 of Ref. 21, where the biases of the MLE obtained from a purely random signal are found to be much larger than those obtained from an equivalent deterministic signal, and range estimation is more severely affected.

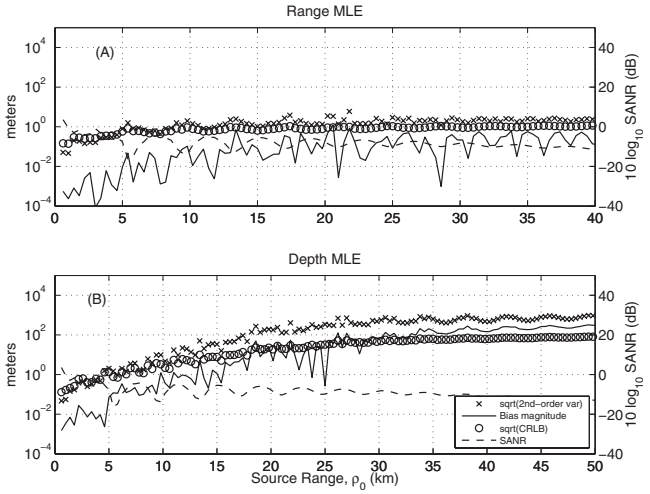

FIG. 10. The same as Fig. 7, but here the covariance **C** of the measurement is assumed parameter independent so that its derivatives in Eqs. (12) and (13) are set to zero. The asymptotic biases and variances of source range and depth MLEs are typically underestimated, as seen by comparing with Fig. 7. This scenario is equivalent to incorrectly assuming the received measurement is a deterministic signal embedded in purely additive white noise, in which case the SANR and SNR of the measurement are equal and the two curves coincide.

Both approximations to the measured signal model are inappropriate for determining the sample sizes required to obtain MLEs of source position that attain desired error thresholds. The minimum errors for unbiased estimates of source position given a single sample are shown in Figs. 12(a) and 12(b) and Figs. 13(a) and 13(b). The sample sizes necessary to attain either of these CRLBs are given in Figs. 12(c) and 12(d) and Figs. 13(c) and 13(d). Setting the derivatives of **C** in Eqs. (12) and (13) to zero results in underestimating the sample size required to obtain an accurate estimate of source range by a factor of typically 10^2, as seen by comparing Figs. 10(a) and 12(a) to Figs. 7(a) and 9(a), *given the SANR*[1] *in Fig. 6(a)*. Similarly, setting instead the derivatives of $\boldsymbol{\mu}$ to zero leads to an overestimation of this sample size by a factor of at least 10^7, *given the SANR*[1] *in Fig. 6(a)*. In the latter case, the degradation in range estimation is especially notable and minimum errors are now at least as large as tens of kilometers beyond 20 km from the source, having increased by several orders of magnitude from those calculated in Sec. III B.

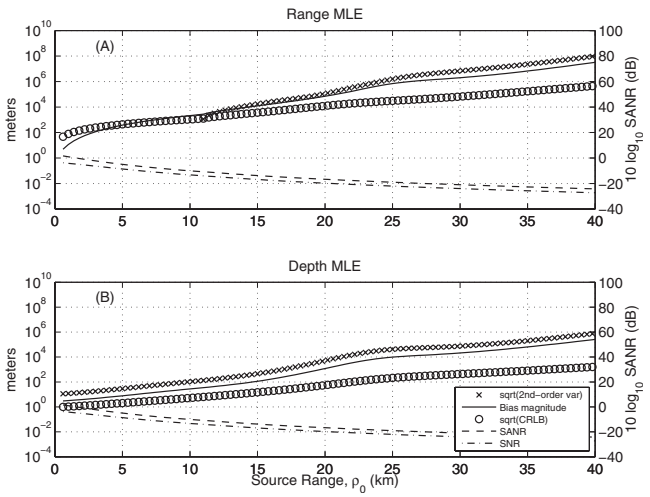

FIG. 11. The same as Fig. 7, but here the mean $\boldsymbol{\mu}$ of the measurement is assumed parameter independent so that its derivatives in Eqs. (12) and (13) are set to zero. The asymptotic biases and variances of source range and depth MLEs may be significantly overestimated, as seen by comparing with Fig. 7. This scenario is equivalent to incorrectly assuming the received measurement is purely random with zero mean, embedded in additive white noise.

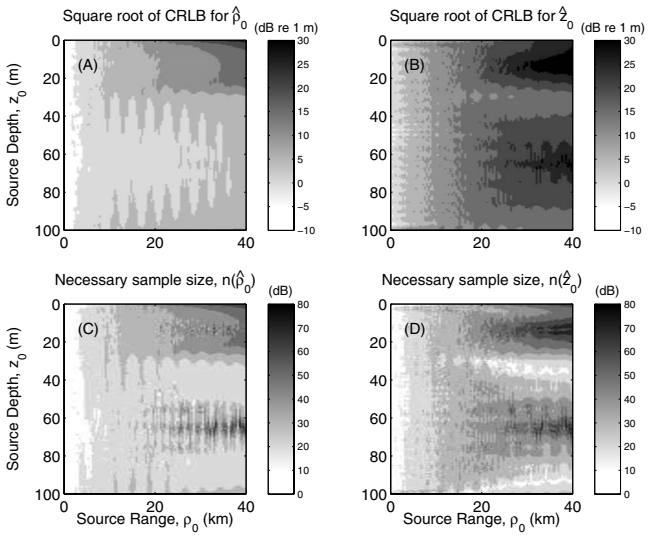

FIG. 12. The same as Fig. 9, but here the covariance **C** of the measurement is assumed parameter independent so that its derivatives in Eqs. (12) and (13) are set to zero. The CRLB and the sample sizes necessary to attain it are underestimated when compared with Fig. 9. This scenario is equivalent to incorrectly assuming the received measurement is a deterministic signal embedded in purely additive white noise.

C. Discussion

We have calculated the sample sizes or SANRs necessary to obtain accurate source localization estimates in a

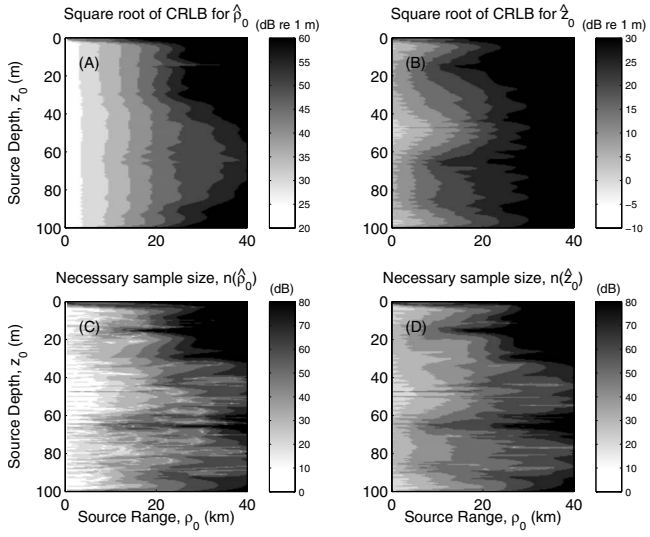

FIG. 13. The same as Fig. 9, but here the mean $\boldsymbol{\mu}$ of the measurement is assumed parameter independent so that its derivatives in Eqs. (12) and (13) are set to zero. The CRLB and the sample sizes necessary to attain it are overestimated when compared with Fig. 9. This scenario is equivalent to incorrectly assuming the received measurement is purely random with zero mean, embedded in additive white noise.

static and a fluctuating waveguide, given a 415 Hz source and an $N/2=10$ element array in Secs. III A and III B. As a rough design rule, we find that in the lower layer of both the undisturbed and fluctuating waveguide, source range can be typically estimated to within $100\times M$ m if the received $10\log_{10}$ SANR at a single hydrophone is at least $(13+10\log_{10}20/N'-20\log_{10}M)$ dB, given a single sample and a vertical array of $N'/2$ elements. The necessary SANRs for both the undisturbed and fluctuating waveguide follow the same design rule because they have similar range-averaged behavior.

The necessary sample sizes or SANRs presented here are consistent with those reported in experimental studies. For example, in Ref. 17, the authors localize a source at a range of 5 km with an accuracy of approximately 200 m using single measurements at similar frequencies as investigated here from a 32-element array, despite uncertainties in the sound speed profile. The effective $10\log_{10}$ SANR of their multi-spectral measurement is roughly 16 dB at a single hydrophone, which is much higher than the $(13+10\log_{10}(10/32)-20\log_{10}2)\approx 2$ dB estimated from our rough design rule for accurate source localization in a fluctuating waveguide.

IV. CONCLUSIONS

A method is provided for determining necessary conditions on sample size or signal to noise ratio (SNR) to obtain accurate parameter estimates from remote sensing measurements in a fluctuating ocean waveguide. These conditions are derived by first expanding the bias and covariance of maximum likelihood estimates (MLEs) in inverse orders of sample size or SNR, where the first-order term in the covariance expansion is the minimum mean square error (MSE) of any unbiased estimate, the Cramer-Rao lower bound (CRLB). Necessary sample sizes or SNRs are then determined by requiring (i) the first-order bias term and the second-order covariance term to be much smaller than the true value of the parameter and the CRLB, respectively, and (ii) the CRLB to fall within desired error thresholds. An analytical expression is provided for the second-order covariance of MLEs obtained from general complex Gaussian data vectors, which can be used in many practical problems since (i) data distributions can often be assumed to be Gaussian by virtue of the central limit theorem, and (ii) it allows for *both* the mean and the variance of the measurement to be functions of the estimation parameters. By comparing the asymptotic biases and errors of MLEs, and the sample sizes or SNRs necessary to attain accurate estimates in a static waveguide and in the presence of internal waves, it is then possible to quantitatively assess the effects of environmental uncertainties on parameter estimation.

Here, we consider the problem of source localization in a fluctuating waveguide containing random internal waves, which we model using the analytical expressions provided in Ref. 5 for the mean, mutual intensity, and spatial covariance of the acoustic field forward propagated through random 3-D internal waves in a stratified ocean waveguide for a continuous wave (CW) narrowband signal. The loss of coherence in the forward propagating field due to scattering by internal waves may have severe consequences on parameter estimation and lead to significant losses in localization ability with narrowband vertical array measurements for fixed source and receiver. We determine the sample sizes and SNRs necessary to obtain accurate source localization estimates in an undisturbed waveguide and find that the median necessary sample size or SNR increases by at least an order magnitude in a fluctuating waveguide, when internal wave fluctuations result in the incoherent intensity component dominating the total acoustic field intensity. Past experiments demonstrating localization with matched-field processing (MFP) in random or fluctuating environments have used SNRs that exceeded the derived conditions and so have not tested the limits of passive detection and localization. In practice, many stealthy or distant sources will have much lower SNRs than have been used in current experiments, and so would likely require impractically long stationary averaging periods for localization to be possible. The results shown here provide an example of how asymptotic statistics can be used in experimental design to ensure that statistical biases and errors meet predetermined error thresholds.

We also demonstrate the advantages of using the expression for the second-order covariance presented here, which accounts for parameter dependence on both the mean and the variance of the measurement. This is achieved by comparing the asymptotic biases and errors to those calculated when either the covariance or the mean of the measurement is incorrectly assumed to be parameter independent. Such approximations are often necessary to model the measured field in fluctuating environments when it is not possible to determine the parameter dependence of both its mean and variance. Using the analytical tools developed here, we can instead take advantage of the parameter dependence of both the mean and variance of the measured field to obtain more accurate parameter estimates. We find that modeling the measurement as a deterministic signal vector leads to significantly underestimating both the CRLB as well as the sample size or SNR required to attain it. Similarly, modeling the measurement as a zero-mean, fully randomized signal vector results in a gross overestimation of the CRLB and the required sample size or SNR to attain it.

APPENDIX A: MEAN, COVARIANCE OF THE FORWARD PROPAGATED FIELD, AND THEIR DERIVATIVES

Here, we review the analytical expressions for the mean field, variance, and expected total intensity of the forward field propagated through an ocean waveguide containing random internal waves. These expressions will be used to calculate the mean vector $\boldsymbol{\mu}$ and the covariance matrix $\mathbf{C}$ in Eq. (11), and determine their derivatives with respect to source range and depth. We employ the formulation developed in Refs. 5 and 41, where it is assumed that the internal wave inhomogeneities follow a stationary random process in space. Referring to Fig. 1, for a source at $\mathbf{r_0}=(-\rho_0,0,z_0)$, the mean forward field received by the qth hydrophone array element at $\mathbf{r}_q=(0,0,z_q)$ is given by Eq. (83) of Ref. 41

$$\langle \Psi_T(\mathbf{r}_q|\mathbf{r}_0)\rangle = \sum_n \Psi_i^{(n)}(\mathbf{r}_q|\mathbf{r}_0) e^{i\int_{-\rho_0}^0 \nu_n(\rho_s)d\rho_s}, \tag{A1}$$

where ρ_s is the horizontal location of the internal wave inhomogeneity, and

$$\Psi_i^{(n)}(\mathbf{r}_q|\mathbf{r}_0) = 4\pi \frac{i}{d(z_0)\sqrt{8\pi}} e^{-i\pi/4} u_n(z_q) u_n(z_0) \frac{e^{i\xi_n\rho_0}}{\sqrt{\xi_n\rho_0}} \tag{A2}$$

is the incident field contribution from mode n given no inhomogeneities in the medium, $d(z_0)$ is the density at the source depth z_0, $u_n(z)$ is the modal amplitude at depth z, ξ_n is the horizontal wave number, and ν_n is the change in the horizontal wave number due to multiple scattering from the inhomogeneities. As detailed in Ref. 41, the modal horizontal wave number change is complex, and it leads to both dispersion and attenuation in the mean forward field. Analytic expressions for ν_n are provided in Eqs. (56) and (60) of Ref. 41 for compact inhomogeneities that obey a stationary random process in depth and for general inhomogeneities with arbitrary depth dependence, respectively.

The variance of the forward field at the receiver is given by Eq. (84) of Ref. 41

$$\begin{aligned} Var(\Psi_T(\mathbf{r}_q|\mathbf{r}_0)) = \sum_n & \frac{2\pi}{d^2(z_0)} \frac{1}{|\xi_n|\rho_0} |u_n(z_0)|^2 |u_n(z_q)|^2 \\ & \times e^{-2\Im\left\{\xi_n\rho_0 + \int_{-\rho_0}^0 \nu_n(\rho_s)d\rho_s\right\}} \\ & \times \left(e^{\int_{-\rho_0}^0 \mu_n(\rho_a)d\rho_a} - 1\right), \end{aligned} \tag{A3}$$

where μ_n is defined in Ref. 41 as the exponential coefficient of modal field variance, and $\Im\{\ldots\}$, $\Re\{\ldots\}$ correspond to the imaginary and real part, respectively. The variance of the forward field depends on the first- and second-order moments of the scatter function density of the random medium. Analytic expressions for μ_n for general surface and volume inhomogeneities are provided in Eqs. (74) and (77) of Ref. 41 for fully correlated and uncorrelated scatterers, respectively.

The covariance of the forward fields received at $\mathbf{r}_q$ and $\mathbf{r}_p$ is given by Eq. (104) of Ref. 41

$$\begin{aligned} &\mathrm{Cov}(\Psi_T(\mathbf{r}_q|\mathbf{r}_0), \Psi_T(\mathbf{r}_p|\mathbf{r}_0)) \\ &= \sum_n \frac{2\pi}{d^2(z_0)} \frac{1}{|\xi_n|\rho_0} |u_n(z_0)|^2 u_n(z_q) u^*(z_p) e^{-2\Im\{\xi_n\}\rho_0} \\ &\times \exp\left(\int_{-\rho_0}^0 (i\Re\{\nu_{n,q}(\rho_s) - \nu_{n,p}(\rho_s)\} - \Im\{\nu_{n,q}(\rho_s) \right. \\ &\left. + \nu_{n,p}(\rho_s)\}) d\rho_s \right) \times \left(e^{\int_{-\rho_0}^0 \mu_{n,q,p}(\rho_s)d\rho_s} - 1\right). \end{aligned} \tag{A4}$$

The mean forward field of Eq. (A1) is also called the coherent field, the magnitude square of which is proportional to coherent intensity. The variance of the forward field in Eq. (A3) provides a measure of the incoherent intensity. The total intensity of the forward field is the sum of the coherent and incoherent intensities. As shown in Ref. 5, the coherent field tends to dominate at short ranges from the source and in slightly random media, while the incoherent field tends to dominate in highly random media. It should be noted that in a nonrandom waveguide $\mu_n = 0$ so that the variance of the forward field is zero, from Eq. (A3). This is expected since the field is fully coherent in this case.

1. Derivatives of the mean field with respect to source range and depth

Going back to Eq. (A1), the modal amplitude $u_n(z)$ is defined as

$$u_n(z) = [N^{(1)} e^{i\Re\{\gamma_n\}z} - N^{(2)} e^{-i\Re\{\gamma_n\}z}] e^{-\Im\{\gamma_n\}z}. \tag{A5}$$

We will assume that

$$\int_{-\rho_0}^0 \nu_n(\rho_s)d\rho_s = \nu_n\rho_0 \tag{A6a}$$

and

$$\frac{\partial d(z_0)}{\partial z_0} = 0, \tag{A6b}$$

so that

$$\langle \Psi_T(\mathbf{r}|\mathbf{r_0})\rangle = \sum_{n=1}^{\infty} C_n(z) f_n(z_0) g_n(\rho_0), \tag{A7}$$

where the following quantities have been defined

$$C_n(z) = 4\pi \frac{i}{d(z_0)\sqrt{8\pi\xi_n}} e^{-i\pi/4} u_n(z), \tag{A8a}$$

$$f_n(z_0) = u_n(z_0), \tag{A8b}$$

$$g_n(\rho_0) = \frac{1}{\sqrt{\rho_0}} e^{i(\xi_n + \nu_n)\rho_0}. \tag{A8c}$$

The derivatives of the mean field with respect to source depth and range can then be simply expressed in terms of derivatives of $f_n(z_0)$, $g_n(\rho_0)$ and their products, respectively.

a. Depth derivatives

The first three derivatives of the mean with respect to source depth z_0 are given by

$$\begin{aligned} f_n^1(z_0) = & i\Re\{\gamma_n\}[N^{(1)} e^{i\Re\{\gamma_n\}z_0} + N^{(2)} e^{-i\Re\{\gamma_n\}z_0}] e^{-\Im\{\gamma_n\}z_0} \\ & - \Im\{\gamma_n\} f_n(z_0), \end{aligned} \tag{A9a}$$

$$f_n^2(z_0) = -[(\Re\{\gamma_n\})^2 + (\Im\{\gamma_n\})^2] f_n(z_0) - 2\Im\{\gamma_n\} f_n^1(z_0), \tag{A9b}$$

$$f_n^3(z_0) = -[(\Re\{\gamma_n\})^2 + (\Im\{\gamma_n\})^2] f_n^1(z_0) - 2\Im\{\gamma_n\} f_n^2(z_0). \tag{A9c}$$

b. Range derivatives

The first three derivatives of the mean with respect to source range ρ_0 are given by

$$g_n^1(\rho_0) = \frac{e^{i(\xi_n + \nu_n)\rho_0}}{\sqrt{\rho_0}} \left(i(\xi_n + \nu_n) - \frac{1}{2\rho_0} \right), \tag{A10a}$$

$$g_n^2(\rho_0) = \frac{e^{i(\xi_n+\nu_n)\rho_0}}{\sqrt{\rho_0}}\left[-(\xi_n+\nu_n)^2 - i\frac{(\xi_n+\nu_n)}{\rho_0} + \frac{3}{4\rho_0^2}\right], \tag{A10b}$$

$$g_n^3(\rho_0) = \frac{e^{i(\xi_n+\nu_n)\rho_0}}{\sqrt{\rho_0}}\left[-(\xi_n+\nu_n)^3 + \frac{3}{2\rho_0}(\xi_n+\nu_n)^2 + i\frac{9}{4\rho_0^2}(\xi_n+\nu_n) - \frac{15}{8\rho_0^3}\right]. \tag{A10c}$$

2. Derivatives of the covariance of the field with respect to source range and depth

We can express the covariance of the forward propagated field in Eq. (A4) as

$$\mathrm{Cov}(\Psi_T(\mathbf{r}_m|\mathbf{r}_0),\Psi_T(\mathbf{r}_p|\mathbf{r}_0)) \equiv \sum_{n=1}^{\infty} D_n(z_m,z_p)h_n(z_0)l_n(\rho_0), \tag{A11}$$

where

$$D_n(z_m,z_p) = \frac{2\pi}{d^2(z_0)|\xi_n|}u_n(z_m)u_n^*(z_p), \tag{A12a}$$

$$h_n(z_0) = |u_n(z_0)|^2, \tag{A12b}$$

$$l_n(\rho_0) = \frac{1}{\rho_0}e^{-2\Im\{\xi_n+\nu_n\}\rho_0}\left(e^{\int_{-\rho_0}^0 \mu_n(\rho_s)d\rho_s} - 1\right). \tag{A12c}$$

We can simplify the above expressions for $h_n(z_0)$ and $l_n(\rho_0)$ by writing

$$h_n(z_0) = (e^{-2\Im\{\gamma_n\}z_0})[\cos^2(\Re\{\gamma_n\}z_0)M1 + \sin^2(\Re\{\gamma_n\}z_0)M2 + 2\cos(\Re\{\gamma_n\}z_0)\sin(\Re\{\gamma_n\}z_0)M3], \tag{A13}$$

and,

$$l_n(\rho_0) = \frac{1}{\rho_0}e^{-2\Im\{\xi_n+\nu_n\}\rho_0}\left(e^{\int_{-\rho_0}^0 \mu_n(\rho_s)d\rho_s} - 1\right) \equiv \frac{1}{\rho_0}e^{-\kappa_n\rho_0}(\lambda_n - 1), \tag{A14}$$

where

$$M1 = (\Re\{N^{(1)} - N^{(2)}\})^2 + (\Im\{N^{(1)} - N^{(2)}\})^2, \tag{A15a}$$

$$M2 = (\Re\{N^{(1)} + N^{(2)}\})^2 + (\Im\{N^{(1)} + N^{(2)}\})^2, \tag{A15b}$$

$$M3 = 2[\Re\{N^{(2)}\}\Im\{N^{(1)}\} - \Re\{N^{(1)}\}\Im\{N^{(2)}\}], \tag{A15c}$$

$$\kappa_n = 2\Im\{\xi_n + \nu_n\}, \tag{A15d}$$

$$\lambda_n = e^{\int_{-\rho_0}^0 \mu_n(\rho_s)d\rho_s}. \tag{A15e}$$

The derivatives of the covariance of the field with respect to source depth and range can then be simply expressed in terms of derivatives of $h_n(z_0)$, $l_n(\rho_0)$ and their products, respectively.

a. Depth derivatives

The first three derivatives of the variance with respect to source depth z_0 are given by

$$h_n^1(z_0) = -2\Im\{\gamma_n\}h_n(z_0) + 2\Re\{\gamma_n\}e^{-2\Im\{\gamma_n\}z_0}[- \cos(\Re\{\gamma_n\}z_0)\sin(\Re\{\gamma_n\}z_0)(M1 - M2) + (\cos^2(\Re\{\gamma_n\}z_0) - \sin^2(\Re\{\gamma_n\}z_0))M3], \tag{A16a}$$

$$h_n^2(z_0) = -2\Im\{\gamma_n\}[2h_n^1(z_0) + 2\Im\{\gamma_n\}h_n(z_0)] + 2(\Re\{\gamma_n\})^2e^{-2\Im\{\gamma_n\}z_0}[(\sin^2(\Re\{\gamma_n\}z_0) - \cos^2(\Re\{\gamma_n\}z_0))(M1 - M2) - 4\cos(\Re\{\gamma_n\}z_0)\sin(\Re\{\gamma_n\}z_0)M3], \tag{A16b}$$

$$h_n^3(z_0) = -2\Im\{\gamma_n\}[3h_n^2(z_0) + 6\Im\{\gamma_n\}h_n^1(z_0) + 4(\Im\{\gamma_n\})^2h_n(z_0)] - 4(\Re\{\gamma_n\})^2[h_n^1(z_0) + 2\Im\{\gamma_n\}h_n(z_0)]. \tag{A16c}$$

b. Range derivatives

The first three derivatives of the variance with respect to source range ρ_0 are given by

$$l_n^1(\rho_0) = \frac{1}{\rho_0}e^{-\kappa_n\rho_0}\left[\kappa_n + \frac{1}{\rho_0} + \lambda_n\left(-\kappa_n - \frac{1}{\rho_0} + \mu_n\right)\right], \tag{A17a}$$

$$l_n^2(\rho_0) = \frac{1}{\rho_0}e^{-\kappa_n\rho_0}\left[-\left(\kappa_n + \frac{1}{\rho_0}\right)^2 - \frac{1}{\rho_0^2} + \lambda_n\left(\left(\kappa_n + \frac{1}{\rho_0}\right)^2 - 2\mu_n\left(\kappa_n + \frac{1}{\rho_0}\right) + \frac{1}{\rho_0^2} + \mu_n^2 + \mu_n'\right)\right], \tag{A17b}$$

$$l_n^3(\rho_0) = \frac{1}{\rho_0}e^{-\kappa_n\rho_0}\left[\left(\kappa_n + \frac{1}{\rho_0}\right)^3 + \frac{3}{\rho_0^2}\left(\kappa_n + \frac{1}{\rho_0}\right) + \frac{2}{\rho_0^3} + \lambda_n\left(-\left(\kappa_n + \frac{1}{\rho_0}\right)^3 + 3\mu_n\left(\kappa_n + \frac{1}{\rho_0}\right)^2 - 3\mu_n^2\left(\kappa_n + \frac{1}{\rho_0}\right) - \frac{3}{\rho_0^2}\left(\kappa_n + \frac{1}{\rho_0}\right) + 3\frac{\mu_n}{\rho_0^2} + \mu_n^3 - \frac{2}{\rho_0^3} - 3\mu_n'\left(\kappa_n + \frac{1}{\rho_0}\right) + 3\mu_n\mu_n' + \mu_n''\right)\right]. \tag{A17c}$$

APPENDIX B: JOINT MOMENTS FOR ASYMPTOTIC GAUSSIAN INFERENCE: GENERAL MULTIVARIATE GAUSSIAN DATA

Before giving the explicit expressions for the first order bias and the second order co-variance, we define the auxiliary quantities

$$N_{ab} = \frac{1}{2}\mathbf{C}^{-1}\boldsymbol{\mu}_{ab} + (\mathbf{C}^{-1})_b\boldsymbol{\mu}_a = \frac{1}{2}\mathbf{C}^{-1}\frac{\partial^2\boldsymbol{\mu}}{\partial\vartheta^a\,\partial\vartheta^b} + \frac{\partial\mathbf{C}^{-1}}{\partial\vartheta^b}\frac{\partial\boldsymbol{\mu}}{\partial\vartheta^a}, \tag{B1a}$$

TABLE I. Definitions of the shorthand notations used in Equations B2b-s. perm(a,b,c) is a shorthand for sum of terms obtained by all permutations of the indices a,b, and c. rot(a,b,c) is a shorthand for the sum of terms obtained by rotating the indices a,b, and c. (a↔b) is a shorthand for the sum of terms with indices a and b interchanged. These shorthand notations are used to write Equations B2b-s in a compact manner.

$A_{a_1,a_2,\ldots,a_m}$,	$\mathrm{perm}(a_1,a_2,\ldots,a_m)$	Add the terms with permutated indexes
$A_{a_1,a_2,\ldots,a_m}$,	$\mathrm{rot}(a_1,a_2,\ldots,a_m)$	Add the terms with rotated indexes
$A_{a_1,a_2,\ldots,a_m}$,	$(a_i \leftrightarrow a_j)$	Add the terms with indexes a_i and a_j inverted

$$M_{abc} = \frac{1}{3}\mathbf{C}^{-1}\boldsymbol{\mu}_{abc} + (\mathbf{C}^{-1})_c\boldsymbol{\mu}_{ab} + (\mathbf{C}^{-1})_{bc}\boldsymbol{\mu}_a = \frac{1}{3}\mathbf{C}^{-1}\frac{\partial^3\boldsymbol{\mu}}{\partial\vartheta^a\,\partial\vartheta^b\,\partial\vartheta^c} + \frac{\partial\mathbf{C}^{-1}}{\partial\vartheta^c}\frac{\partial^2\boldsymbol{\mu}}{\partial\vartheta^a\,\partial\vartheta^b} + \frac{\partial^2\mathbf{C}^{-1}}{\partial\vartheta^b\,\partial\vartheta^c}\frac{\partial\boldsymbol{\mu}}{\partial\vartheta^a}, \tag{B1b}$$

$$\check{\mathbf{C}}_{a_1..a_p} = \mathbf{C}^{-1}\mathbf{C}_{a_1..a_p} = \mathbf{C}^{-1}\frac{\partial^p\mathbf{C}}{\partial\vartheta^{a_1}\ldots\partial\vartheta^{a_p}}, \tag{B1c}$$

$$\widetilde{\mathbf{C}}_{a_1..a_p} = \mathbf{C}(\mathbf{C}^{-1})_{a_1..a_p} = \mathbf{C}\frac{\partial^p\mathbf{C}^{-1}}{\partial\vartheta^{a_1}\ldots\partial\vartheta^{a_p}}, \tag{B1d}$$

$$\beta_{abc} = tr\left(\frac{\partial^2}{\partial\vartheta^b\,\partial\vartheta^c}\left[\mathbf{C}^{-1}\frac{\partial\mathbf{C}}{\partial\vartheta^a}\right]\right) + tr\left(\mathbf{C}\frac{\partial^3\mathbf{C}^{-1}}{\partial\vartheta^a\,\partial\vartheta^b\,\partial\vartheta^c}\right), \tag{B1e}$$

and specify that we will write the tensors as a principal group of terms plus the terms obtained by a rearrangement of the indexes using the notation described in Table I. If more than one of the symmetry prescriptions appear in the same tensor, it means that the total number of terms contained is the product of the number of terms generated by each symmetry. As a reminder, for the terms where the sample size n is not explicitly shown, we write a square bracket beside it containing the corresponding power. For example, $v_{ab}v_{cd}[2]$ is proportional to n^2 since it is the product of two terms proportional to n.

The tensors are then given by

$$v_{a,b} = -v_{ab} = \mathbf{i}_{ab} = n\left[\boldsymbol{\mu}_a^T\mathbf{C}^{-1}\boldsymbol{\mu}_b + \tfrac{1}{2}tr(\check{\mathbf{C}}_a\check{\mathbf{C}}_b)\right], \tag{B2a}$$

$$v_{abc} = n\left[-\boldsymbol{\mu}_{ab}^T\mathbf{C}^{-1}\boldsymbol{\mu}_c - \boldsymbol{\mu}_a^T(\mathbf{C}^{-1})_b\boldsymbol{\mu}_c + \tfrac{2}{3}tr(\check{\mathbf{C}}_a\check{\mathbf{C}}_b\check{\mathbf{C}}_c) - \tfrac{1}{2}tr(\check{\mathbf{C}}_{ab}\check{\mathbf{C}}_c)\right],\ \mathrm{rot}(a,b,c), \tag{B2b}$$

$$v_{ab,c} = n\left[N_{ab}{}^T\boldsymbol{\mu}_c + \tfrac{1}{4}tr(\widetilde{\mathbf{C}}_{ab}\widetilde{\mathbf{C}}_c)\right],\ (a\leftrightarrow b), \tag{B2c}$$

$$v_{a,b,c} = n\left[-\tfrac{1}{2}\boldsymbol{\mu}_a^T(\mathbf{C}^{-1})_b\boldsymbol{\mu}_c + \tfrac{1}{6}tr(\check{\mathbf{C}}_a\check{\mathbf{C}}_b\check{\mathbf{C}}_c)\right],\ \mathrm{perm}(a,b,c), \tag{B2d}$$

$$v_{abcd} = n\Big[-\tfrac{1}{8}\boldsymbol{\mu}_{ab}^T\mathbf{C}^{-1}\boldsymbol{\mu}_{cd} - \tfrac{1}{6}\boldsymbol{\mu}_{abc}^T\mathbf{C}^{-1}\boldsymbol{\mu}_d - \tfrac{3}{8}tr(\check{\mathbf{C}}_a\check{\mathbf{C}}_b\check{\mathbf{C}}_c\check{\mathbf{C}}_d) + \tfrac{1}{2}tr(\check{\mathbf{C}}_{ab}\check{\mathbf{C}}_c\check{\mathbf{C}}_d) - \tfrac{1}{16}tr(\check{\mathbf{C}}_{ab}\check{\mathbf{C}}_{cd}) - \tfrac{1}{12}tr(\check{\mathbf{C}}_{abc}\check{\mathbf{C}}_d) - \tfrac{1}{2}\boldsymbol{\mu}_{ab}^T(\mathbf{C}^{-1})_c\boldsymbol{\mu}_d - \tfrac{1}{4}\boldsymbol{\mu}_a^T(\mathbf{C}^{-1})_{bc}\boldsymbol{\mu}_d\Big],\quad \mathrm{perm}(a,b,c,d), \tag{B2e}$$

$$v_{a,b,c,d} = \tfrac{1}{8}v_{a,b}v_{c,d}[2] + n\Big[\tfrac{1}{2}\boldsymbol{\mu}_a^T\mathbf{C}^{-1}\widetilde{\mathbf{C}}_b\widetilde{\mathbf{C}}_c\boldsymbol{\mu}_d + \tfrac{1}{8}tr(\check{\mathbf{C}}_a\check{\mathbf{C}}_b\check{\mathbf{C}}_c\check{\mathbf{C}}_d)\Big],\quad \mathrm{perm}(a,b,c,d), \tag{B2f}$$

$$v_{ab,c,d} = \tfrac{1}{4}v_{ab}v_{c,d}[2] - n\Big[\tfrac{1}{8}tr(\widetilde{\mathbf{C}}_c\widetilde{\mathbf{C}}_d\widetilde{\mathbf{C}}_{ab}) + \tfrac{1}{8}tr(\widetilde{\mathbf{C}}_c\widetilde{\mathbf{C}}_{ab}\widetilde{\mathbf{C}}_d) + N_{ab}{}^T\widetilde{\mathbf{C}}_d\boldsymbol{\mu}_c + \tfrac{1}{4}\boldsymbol{\mu}_c^T\mathbf{C}^{-1}\widetilde{\mathbf{C}}_{ab}\boldsymbol{\mu}_d\Big],\quad (a\leftrightarrow b)(c\leftrightarrow d), \tag{B2g}$$

$$v_{ab,cd} = \tfrac{1}{4}v_{ab}v_{cd}[2] + n\Big[\tfrac{1}{8}tr(\widetilde{\mathbf{C}}_{ab}\widetilde{\mathbf{C}}_{cd}) + N_{ab}{}^T\mathbf{C}N_{cd}\Big],\quad (a\leftrightarrow b)(c\leftrightarrow d), \tag{B2h}$$

$$v_{abc,d} = n\Big[\tfrac{1}{6}tr(\widetilde{\mathbf{C}}_{abc}\widetilde{\mathbf{C}}_d) + M_{abc}^T\boldsymbol{\mu}_d\Big],\quad \mathrm{rot}(a,b,c), \tag{B2i}$$

$$v_{abcde} = n\Big[-\tfrac{1}{24}\boldsymbol{\mu}_{abcd}^T\mathbf{C}^{-1}\boldsymbol{\mu}_e - \tfrac{1}{12}\boldsymbol{\mu}_{abc}^T\mathbf{C}^{-1}\boldsymbol{\mu}_{de} - \tfrac{1}{48}tr(\check{\mathbf{C}}_{abcd}\check{\mathbf{C}}_e) - \tfrac{1}{24}tr(\check{\mathbf{C}}_{abc}\check{\mathbf{C}}_{de}) + \tfrac{1}{6}tr(\check{\mathbf{C}}_{abc}\check{\mathbf{C}}_d\check{\mathbf{C}}_e) + \tfrac{1}{4}tr(\check{\mathbf{C}}_{ab}\check{\mathbf{C}}_{cd}\check{\mathbf{C}}_e) - \tfrac{3}{4}tr(\check{\mathbf{C}}_{ae}\check{\mathbf{C}}_b\check{\mathbf{C}}_c\check{\mathbf{C}}_d) + \tfrac{2}{5}tr(\check{\mathbf{C}}_a\check{\mathbf{C}}_b\check{\mathbf{C}}_c\check{\mathbf{C}}_d\check{\mathbf{C}}_e) - \tfrac{1}{12}\boldsymbol{\mu}_a^T(\mathbf{C}^{-1})_{bcd}\boldsymbol{\mu}_e - \tfrac{1}{8}\boldsymbol{\mu}_{ab}^T\mathbf{C}^{-1}\widetilde{\mathbf{C}}_c\boldsymbol{\mu}_{de} - \tfrac{1}{6}\boldsymbol{\mu}_{abc}^T\mathbf{C}^{-1}\widetilde{\mathbf{C}}_d\boldsymbol{\mu}_e - \tfrac{1}{4}\boldsymbol{\mu}_{ab}^T\mathbf{C}^{-1}\widetilde{\mathbf{C}}_{cd}\boldsymbol{\mu}_e\Big],\quad \mathrm{perm}(a,b,c,d,e), \tag{B2j}$$

$$v_{abc,d,e} = \tfrac{1}{6}v_{d,e}v_{abc}[2] - n\Big[\tfrac{1}{6}tr(\widetilde{\mathbf{C}}_{abc}\widetilde{\mathbf{C}}_d\widetilde{\mathbf{C}}_e) + \tfrac{1}{6}\boldsymbol{\mu}_d^T\mathbf{C}^{-1}\widetilde{\mathbf{C}}_{abc}\boldsymbol{\mu}_e + M_{abc}^T\widetilde{\mathbf{C}}_e\boldsymbol{\mu}_d\Big],\quad \mathrm{rot}(a,b,c)(d\leftrightarrow e), \tag{B2k}$$

$$v_{abc,de} = \tfrac{1}{6}v_{de}v_{abc}[2] + n\Big[\tfrac{1}{12}tr(\widetilde{\mathbf{C}}_{abc}\widetilde{\mathbf{C}}_{de}) + M_{abc}^T\mathbf{C}N_{de}\Big],\quad \mathrm{rot}(a,b,c)(d\leftrightarrow e), \tag{B2l}$$

$$v_{ab,cd,e} = \tfrac{1}{4}v_{ab}v_{cd,e}[2] - \frac{n}{2}\Big[\tfrac{1}{4}tr(\widetilde{\mathbf{C}}_{ab}\widetilde{\mathbf{C}}_e\widetilde{\mathbf{C}}_{cd}) + N_{ab}{}^T\widetilde{\mathbf{C}}_{cd}\boldsymbol{\mu}_e + N_{ab}{}^T\widetilde{\mathbf{C}}_e\mathbf{C}N_{cd}\Big],\quad (a\leftrightarrow b)(c\leftrightarrow d)(ab\leftrightarrow cd), \tag{B2m}$$

$$v_{ab,c,d,e} = \left(\frac{1}{12}v_{ab}v_{c,d,e} + \frac{1}{4}v_{d,e}v_{ab,c}\right)[2] + \frac{n}{2}\left[\frac{1}{2}tr(\tilde{\mathbf{C}}_{ab}\tilde{\mathbf{C}}_c\tilde{\mathbf{C}}_d\tilde{\mathbf{C}}_e) + 2N_{ab}{}^T\tilde{\mathbf{C}}_e\tilde{\mathbf{C}}_c\boldsymbol{\mu}_d + \boldsymbol{\mu}_d^T\mathbf{C}^{-1}\tilde{\mathbf{C}}_c\tilde{\mathbf{C}}_{ab}\boldsymbol{\mu}_e\right], \quad (a \leftrightarrow b)\mathrm{perm}(c,d,e), \tag{B2n}$$

$$v_{abc,d,e,f} = \left(\frac{1}{18}v_{abc}v_{d,e,f} + \frac{1}{6}v_{abc,d}v_{e,f}\right)[2] + \frac{n}{6}[tr(\tilde{\mathbf{C}}_{abc}\tilde{\mathbf{C}}_d\tilde{\mathbf{C}}_e\tilde{\mathbf{C}}_f) + 6M_{abc}^T\tilde{\mathbf{C}}_e\tilde{\mathbf{C}}_f\boldsymbol{\mu}_d + \boldsymbol{\mu}_d^T\mathbf{C}^{-1}\tilde{\mathbf{C}}_f\tilde{\mathbf{C}}_{abc}\boldsymbol{\mu}_e + \boldsymbol{\mu}_d^T\mathbf{C}^{-1}\tilde{\mathbf{C}}_{abc}\tilde{\mathbf{C}}_f\boldsymbol{\mu}_e], \quad \mathrm{rot}(a,b,c)\mathrm{perm}(d,e,f), \tag{B2o}$$

$$v_{ab,cd,e,f} = \frac{1}{16}v_{ab}v_{cd}v_{e,f}[3] + \left(\frac{v_{ab}}{8}(v_{cd,e,f} - v_{cd}v_{e,f}) + \frac{v_{e,f}}{16}(v_{cd,ab} - v_{cd}v_{ab}) + \frac{1}{8}v_{ab,e}v_{cd,f}\right)[2] + n\left[\frac{3}{16}tr(\tilde{\mathbf{C}}_{ab}\tilde{\mathbf{C}}_{cd}\tilde{\mathbf{C}}_e\tilde{\mathbf{C}}_f) + \frac{1}{2}N_{cd}^T\tilde{\mathbf{C}}_e\tilde{\mathbf{C}}_f\mathbf{C}N_{ab} + \frac{1}{8}\boldsymbol{\mu}_d{}^T\mathbf{C}^{-1}\tilde{\mathbf{C}}_{ab}\tilde{\mathbf{C}}_{cd}\boldsymbol{\mu}_f + \boldsymbol{\mu}_e{}^T\mathbf{C}^{-1}\tilde{\mathbf{C}}_f\tilde{\mathbf{C}}_{cd}\mathbf{C}N_{ab}\right], \quad (a \leftrightarrow b)(c \leftrightarrow b)(e \leftrightarrow f)(ab \leftrightarrow cd), \tag{B2p}$$

$$v_{ab,cd,ef,g} = \frac{v_{ab}v_{cd}v_{ef,g}}{16}[3] + \frac{v_{ab}v_{cd,ef,g} + v_{ab,g}v_{ef,cd} - 3v_{ab,g}v_{cd}v_{ef}}{16}[2] + \frac{n}{4}\left[\frac{1}{4}tr(\tilde{\mathbf{C}}_{ab}\tilde{\mathbf{C}}_{cd}\tilde{\mathbf{C}}_{ef}\tilde{\mathbf{C}}_g) + N_{ab}^T\tilde{\mathbf{C}}_{cd}\tilde{\mathbf{C}}_{ef}\boldsymbol{\mu}_g + N_{ab}^T\tilde{\mathbf{C}}_{cd}\tilde{\mathbf{C}}_g\mathbf{C}N_{ef} + N_{ab}^T\tilde{\mathbf{C}}_g\tilde{\mathbf{C}}_{cd}\mathbf{C}N_{ef}\right], \quad (a \leftrightarrow b)(c \leftrightarrow d)(e \leftrightarrow f)\mathrm{perm}(ab,cd,ef), \tag{B2q}$$

$$v_{abcd,e,f,g} = \left(\frac{v_{abcd}v_{e,f,g}}{144} + \frac{v_{abcd,g}v_{e,f}}{48}\right)[2] + n\left[\frac{1}{48}tr(\tilde{\mathbf{C}}_e\tilde{\mathbf{C}}_f\tilde{\mathbf{C}}_g\tilde{\mathbf{C}}_{abcd}) + \left[\frac{1}{6}\boldsymbol{\mu}_a^T\mathbf{C}^{-1}\tilde{\mathbf{C}}_{bcd} + \frac{1}{6}\boldsymbol{\mu}_{abc}^T\mathbf{C}^{-1}\tilde{\mathbf{C}}_d + \frac{1}{4}\boldsymbol{\mu}_{ab}^T\mathbf{C}^{-1}\tilde{\mathbf{C}}_{cd} + \frac{1}{24}\boldsymbol{\mu}_{abcd}^T\mathbf{C}^{-1}\right]\tilde{\mathbf{C}}_e\tilde{\mathbf{C}}_f\boldsymbol{\mu}_g + \frac{1}{24}\boldsymbol{\mu}_e^T\mathbf{C}^{-1}\tilde{\mathbf{C}}_{abcd}\tilde{\mathbf{C}}_f\boldsymbol{\mu}_g\right], \quad \mathrm{perm}(a,b,c,d)\mathrm{perm}(g,e,f), \tag{B2r}$$

$$v_{abc,de,f,g} = \frac{v_{abc}v_{de}v_{f,g}}{12}[3] + \frac{v_{de}v_{abc,f,g} + v_{abc}v_{de,f,g} + v_{f,g}v_{abc,de} + 2v_{abc,f}v_{de,g}}{12}[2] - \frac{v_{de}v_{abc}v_{f,g}}{4}[2] + n\left[M_{abc}^T\tilde{\mathbf{C}}_f\tilde{\mathbf{C}}_g\mathbf{C}N_{de} + \frac{1}{3}N_{de}{}^T\tilde{\mathbf{C}}_f\tilde{\mathbf{C}}_{abc}\boldsymbol{\mu}_g + \frac{1}{3}N_{de}{}^T\tilde{\mathbf{C}}_{abc}\tilde{\mathbf{C}}_f\boldsymbol{\mu}_g + \frac{1}{6}\boldsymbol{\mu}_f^T\mathbf{C}^{-1}\tilde{\mathbf{C}}_{abc}\tilde{\mathbf{C}}_{de}\boldsymbol{\mu}_g + \frac{1}{6}\boldsymbol{\mu}_f^T\mathbf{C}^{-1}\tilde{\mathbf{C}}_{de}\tilde{\mathbf{C}}_{abc}\boldsymbol{\mu}_g + \frac{1}{2}M_{abc}^T\tilde{\mathbf{C}}_{de}\tilde{\mathbf{C}}_f\boldsymbol{\mu}_g + \frac{1}{2}M_{abc}^T\tilde{\mathbf{C}}_f\tilde{\mathbf{C}}_{de}\boldsymbol{\mu}_g + \frac{1}{4}tr(\tilde{\mathbf{C}}_{abc}\tilde{\mathbf{C}}_{de}\tilde{\mathbf{C}}_f\tilde{\mathbf{C}}_g)\right], \quad \mathrm{rot}(a,b,c)(f \leftrightarrow g)(d \leftrightarrow e). \tag{B2s}$$

The expressions given above are in a form suitable for analyzing situations where the parametric dependence is on both the mean vector $\boldsymbol{\mu}$ and the covariance matrix $\mathbf{C}$. The formalism can also be readily adapted to the case where only the mean vector or the covariance depends on the parameters by setting the derivatives of the covariance matrix or the mean vector to zero, respectively.

The explicit expressions of the tensors evaluated for general Gaussian random variables can also be used for random data that are not distributed in a Gaussian form provided that they can be expressed as functions of Gaussian random variables with a Jacobian of the transformation that is independent of the parameters to be estimated.[30] Consider for example a single vector sample composed of $R_1, \ldots, R_b$ arbitrary random variables which can be expressed in terms of $y_1, \ldots, y_q$ Gaussian random variables ($q \geq b$). Assume the Jacobian of the transformation is independent of the m-dimensional parameter vector $\boldsymbol{\theta}$. The mapping is assumed to be one-to-one between $\mathbf{y} = [y_1, \ldots, y_q]^T$ and $\mathbf{R} = [R_1, \ldots, R_b]^T$ (for $q = b$), or between $\mathbf{y}$ and $\mathbf{R}' \equiv [\mathbf{R}, \boldsymbol{\Omega}]^T \equiv [R_1, \ldots, R_b, \Omega_1, \ldots, \Omega_{q-b}]^T$ (for $q > b$), with $\Omega_1, \ldots, \Omega_{q-b}$ some arbitrary random variables that are not dependent on the parameter vector $\boldsymbol{\theta}$. For the general case of $q > b$, the parameter independent Jacobian of the transformation is $J' = |\partial \mathbf{y} / \partial \mathbf{R}'|$. Under these assumptions, we have the following identity which holds for the expectation of any function of derivatives of the likelihood function with respect to the parameters,[30]

$$\langle f \rangle_{\mathbf{R}} = \int f\left(\frac{\partial\, ln(p(\mathbf{R}|\boldsymbol{\theta}))}{\partial \theta_i}, \cdots, \frac{\partial^d\, ln(p(\mathbf{R}|\boldsymbol{\theta}))}{\partial \theta_i^d}\right) p(\mathbf{R}|\boldsymbol{\theta})\mathrm{d}\mathbf{R} = \int\int f\left(\frac{\partial\, ln(p(\mathbf{R}|\boldsymbol{\theta})p(\boldsymbol{\Omega}))}{\partial \theta_i}, \cdots, \frac{\partial^d\, ln(p(\mathbf{R}|\boldsymbol{\theta})p(\boldsymbol{\Omega}))}{\partial \theta_i^d}\right) \times p(\mathbf{R}|\boldsymbol{\theta})p(\boldsymbol{\Omega})\mathrm{d}\mathbf{R}\mathrm{d}\boldsymbol{\Omega}, \tag{B3}$$

for all $i=1,2,\ldots,m$, where the last equality is introduced so as to make the transformation between $\mathbf{R}'$ and $\mathbf{y}$, since $p(\mathbf{R}|\boldsymbol{\theta})p(\boldsymbol{\Omega})=p(\mathbf{y}(\mathbf{R},\boldsymbol{\Omega}|\boldsymbol{\theta}))J'$ and $\boldsymbol{\Omega}$ is parameter independent. Equation (B3) can then be written as

$$\begin{aligned}\langle f\rangle_{\mathbf{R}} &= \int\int f\left(\frac{\partial\, ln(p(\mathbf{y}(\mathbf{R},\boldsymbol{\Omega})|\boldsymbol{\theta})J')}{\partial\theta_i},\cdots,\right.\\ &\left.\frac{\partial^d\, ln(p(\mathbf{x}(\mathbf{R},\boldsymbol{\Omega})|\boldsymbol{\theta})J')}{\partial\theta_i^d}\right)\\ &\times p(\mathbf{y}(\mathbf{R},\boldsymbol{\Omega})|\boldsymbol{\theta})J'\mathrm{d}\mathbf{R}\mathrm{d}\boldsymbol{\Omega}\\ &= \int f\left(\frac{\partial\, ln(p(\mathbf{y}|\boldsymbol{\theta}))}{\partial\theta_i},\cdots,\frac{\partial^d\, ln(p(\mathbf{y}|\boldsymbol{\theta}))}{\partial\theta_i^d}\right)p(\mathbf{y}|\boldsymbol{\theta})\mathrm{d}\mathbf{y}\\ &= \langle f\rangle_{\mathbf{y}}. \end{aligned} \tag{B4}$$

The expected value of any function of derivatives of the likelihood function for $\mathbf{R}$ with respect to the parameters $\boldsymbol{\theta}$ can then be written as the same function of derivatives of the likelihood function for $\mathbf{y}$. Since the asymptotic orders are function of expectations that have the same structure as Eq. (B3), the asymptotic orders of the MLE of a parameter $\boldsymbol{\theta}$ can be computed from measurements of the non-Gaussian quantity $\mathbf{R}$.

For example, the MLE of a scalar parameter θ from an observation R distributed as a Gamma with parameter dependent mean $\sigma(\theta)$,

$$p(R|\theta)=\left(\frac{n}{\sigma(\theta)}\right)^n\frac{R^{n-1}}{\Gamma(n)}\exp\left(-\frac{nR}{\sigma(\theta)}\right), \tag{B5}$$

can be computed using the set of Gaussian random variables $y_1,\ldots,y_{2n}$

$$p(y_1,\ldots,y_{2n}|\theta)=\prod_{i=1}^{2n}\frac{1}{\sqrt{\pi\sigma(\theta)}}\exp\left(-\frac{y_i^2}{\sigma(\theta)}\right). \tag{B6}$$

Substituting for the tensors of Eq. (B2) into Eqs. (8) and (10), expressions are obtained for the first-order bias and second-order covariance of the MLE given general multivariate Gaussian data. The former has been stated in Eq. (7) of Ref. 1, while the latter is now shown here. For the diagonal terms of the second order covariance matrix,

$$\begin{aligned} var_2(\hat{\theta}^r,\hat{\theta}^r) = {} & i^{rr}+i^{rm}i^{rm}i^{ab}\Big[\boldsymbol{\mu}_{ma}\mathbf{C}^{-1}\boldsymbol{\mu}_{mb}-\boldsymbol{\mu}_{mm}\mathbf{C}^{-1}\boldsymbol{\mu}_{ab}-\boldsymbol{\mu}_{mab}\mathbf{C}^{-1}\boldsymbol{\mu}_{m}+tr(\check{\mathbf{C}}_m\check{\mathbf{C}}_m\check{\mathbf{C}}_a\check{\mathbf{C}}_b)+tr(\check{\mathbf{C}}_m\check{\mathbf{C}}_a\check{\mathbf{C}}_m\check{\mathbf{C}}_b)\\ & +tr(\check{\mathbf{C}}_{ab}\check{\mathbf{C}}_m\check{\mathbf{C}}_m)-tr(\check{\mathbf{C}}_{ma}\check{\mathbf{C}}_m\check{\mathbf{C}}_b)-tr(\check{\mathbf{C}}_{ma}\check{\mathbf{C}}_b\check{\mathbf{C}}_m)+\tfrac{1}{2}tr(\check{\mathbf{C}}_{ma}\check{\mathbf{C}}_{mb})-\tfrac{1}{2}tr(\check{\mathbf{C}}_{mm}\check{\mathbf{C}}_{ab})-\tfrac{1}{2}tr(\check{\mathbf{C}}_{mab}\check{\mathbf{C}}_m)\\ & +4\boldsymbol{\mu}_{ma}(\mathbf{C}^{-1})_m\boldsymbol{\mu}_b+2\boldsymbol{\mu}_{ma}(\mathbf{C}^{-1})_b\boldsymbol{\mu}_m-\boldsymbol{\mu}_{ab}(\mathbf{C}^{-1})_m\boldsymbol{\mu}_m+\boldsymbol{\mu}_a(\mathbf{C}^{-1})_{mm}\boldsymbol{\mu}_b+\boldsymbol{\mu}_m(\mathbf{C}^{-1})_a(\mathbf{C}^{-1})_b\boldsymbol{\mu}_m\\ & +2\boldsymbol{\mu}_m(\mathbf{C}^{-1})_a(\mathbf{C}^{-1})_m\boldsymbol{\mu}_b+\boldsymbol{\mu}_a(\mathbf{C}^{-1})_m(\mathbf{C}^{-1})_m\boldsymbol{\mu}_b\Big]+i^{rm}i^{rm}i^{ab}i^{cd}\Big\{\boldsymbol{\mu}_{ma}\mathbf{C}^{-1}\boldsymbol{\mu}_c[-\boldsymbol{\mu}_{md}\mathbf{C}^{-1}\boldsymbol{\mu}_b-2\boldsymbol{\mu}_b(\mathbf{C}^{-1})_d\boldsymbol{\mu}_m\\ & -4\boldsymbol{\mu}_b(\mathbf{C}^{-1})_m\boldsymbol{\mu}_d-tr(\check{\mathbf{C}}_{md}\check{\mathbf{C}}_b)+tr(\check{\mathbf{C}}_{bd}\check{\mathbf{C}}_m)+tr(\check{\mathbf{C}}_m\check{\mathbf{C}}_b\check{\mathbf{C}}_d)+tr(\check{\mathbf{C}}_m\check{\mathbf{C}}_d\check{\mathbf{C}}_b)]+\boldsymbol{\mu}_{ac}\mathbf{C}^{-1}\boldsymbol{\mu}_m\Big[\tfrac{1}{2}\boldsymbol{\mu}_{bd}\mathbf{C}^{-1}\boldsymbol{\mu}_m\\ & +2\boldsymbol{\mu}_{mb}\mathbf{C}^{-1}\boldsymbol{\mu}_d+\tfrac{1}{2}tr(\check{\mathbf{C}}_{bd}\check{\mathbf{C}}_m)+tr(\check{\mathbf{C}}_{mb}\check{\mathbf{C}}_d)-tr(\check{\mathbf{C}}_m\check{\mathbf{C}}_b\check{\mathbf{C}}_d)\Big]+tr(\check{\mathbf{C}}_m\check{\mathbf{C}}_a\check{\mathbf{C}}_c)\Big[\boldsymbol{\mu}_m(\mathbf{C}^{-1})_b\boldsymbol{\mu}_d+\boldsymbol{\mu}_m(\mathbf{C}^{-1})_d\boldsymbol{\mu}_b\\ & +3\boldsymbol{\mu}_b(\mathbf{C}^{-1})_m\boldsymbol{\mu}_d+\tfrac{1}{2}(-tr(\check{\mathbf{C}}_m\check{\mathbf{C}}_b\check{\mathbf{C}}_d)-tr(\check{\mathbf{C}}_m\check{\mathbf{C}}_d\check{\mathbf{C}}_b)+tr(\check{\mathbf{C}}_{md}\check{\mathbf{C}}_b)+tr(\check{\mathbf{C}}_{mb}\check{\mathbf{C}}_d)-tr(\check{\mathbf{C}}_{bd}\check{\mathbf{C}}_m))\Big]+tr(\check{\mathbf{C}}_{ma}\check{\mathbf{C}}_c)\\ & \times\Big[-\tfrac{1}{4}tr(\check{\mathbf{C}}_{md}\check{\mathbf{C}}_b)-\boldsymbol{\mu}_m(\mathbf{C}^{-1})_d\boldsymbol{\mu}_b-2\boldsymbol{\mu}_b(\mathbf{C}^{-1})_m\boldsymbol{\mu}_d\Big]-\tfrac{3}{2}\boldsymbol{\mu}_a(\mathbf{C}^{-1})_m\boldsymbol{\mu}_c\boldsymbol{\mu}_b(\mathbf{C}^{-1})_m\boldsymbol{\mu}_d+tr(\check{\mathbf{C}}_{ac}\check{\mathbf{C}}_m)\Big[\tfrac{1}{2}tr(\check{\mathbf{C}}_{mb}\check{\mathbf{C}}_d)\\ & +\tfrac{1}{8}tr(\check{\mathbf{C}}_{bd}\check{\mathbf{C}}_m)\Big]+\boldsymbol{\mu}_m(\mathbf{C}^{-1})_a\boldsymbol{\mu}_c[-\boldsymbol{\mu}_m(\mathbf{C}^{-1})_d\boldsymbol{\mu}_b-2\boldsymbol{\mu}_b(\mathbf{C}^{-1})_m\boldsymbol{\mu}_d]+\Big[\boldsymbol{\mu}_{cd}\mathbf{C}^{-1}\boldsymbol{\mu}_a-\boldsymbol{\mu}_c(\mathbf{C}^{-1})_a\boldsymbol{\mu}_d+\tfrac{1}{2}tr(\check{\mathbf{C}}_{cd}\check{\mathbf{C}}_a)\Big]\\ & \times\Big[\tfrac{1}{2}tr(\check{\mathbf{C}}_{mm}\check{\mathbf{C}}_b)+\tfrac{1}{2}tr(\check{\mathbf{C}}_{mb}\check{\mathbf{C}}_m)-tr(\check{\mathbf{C}}_m\check{\mathbf{C}}_m\check{\mathbf{C}}_b)+\boldsymbol{\mu}_{mm}\mathbf{C}^{-1}\boldsymbol{\mu}_b+\boldsymbol{\mu}_{mb}\mathbf{C}^{-1}\boldsymbol{\mu}_m+\boldsymbol{\mu}_m(\mathbf{C}^{-1})_m\boldsymbol{\mu}_b\Big]\Big\}. \end{aligned} \tag{B7}$$

[1] E. Naftali and N. C. Makris, "Necessary conditions for a maximum likelihood estimate to become asymptotically unbiased and attain the Cramer-Rao lower bound. Part I. General approach with an application to time-delay and Doppler shift estimation," J. Acoust. Soc. Am. **110**, 1917–1930 (2001).

[2] L. L. V. Trees, *Detection, Estimation and Modulation Theory* (Wiley, New York, 1970), Vol. **3**, Chap. 6.

[3] J. W. Goodman, *Statistical Optics* (Wiley, New York, 1985), Chap. 6.

[4] *Full Field Inversion Methods in Ocean and Seismic Acoustics*, edited by O. Diachok, A. Caiti, P. Gerstoft, and H. Schmidt (Kluwer, Dordrecht, 1995), pp. 235–401.

[5] T. Chen, P. Ratilal, and N. C. Makris, "Mean and variance of the forward field propagated through three-dimensional random internal waves in a continental-shelf waveguide," J. Acoust. Soc. Am. **118**, 3560–3574 (2005).

[6] A. B. Baggeroer, W. A. Kuperman, and H. Schmidt, "Matched field processing: Source localization in correlated noise as an optimum parameter estimation problem," J. Acoust. Soc. Am. **83**, 571–587 (1988).

[7] A. B. Baggeroer, W. A. Kuperman, and P. N. Mikhalevsky, "An overview of matched field methods in ocean acoustics," IEEE J. Ocean. Eng. **18**, 401–424 (1993).

[8] M. D. Collins and W. A. Kuperman, "Focalization: Environmental focusing and source localization," J. Acoust. Soc. Am. **90**, 1410–1422 (1991).

[9] A. Tolstoy, "Sensitivity of matched field processing to sound speed profile mismatch for vertical arrays in a deep water pacific environment," J. Acoust. Soc. Am. **85**, 2394–2404 (1989).

[10] D. F. Gingras, "Methods for predicting the sensitivity of matched-field processors to mismatch," J. Acoust. Soc. Am. **86**, 1940–1949 (1989).

[11] G. B. Smith, H. A. Chandler, and C. Feuillade, "Performance stability of high-resolution matched-field processors to sound-speed mismatch in a shallow-water environment," J. Acoust. Soc. Am. **93**, 2617–2626 (1993).

[12] L. T. Fialkowski, M. D. Collins, J. S. Perkins, and W. A. Kuperman, "Source localization in noisy and uncertain ocean environments," J. Acoust. Soc. Am. **101**, 3539–3545 (1997).

[13] H. Schmidt, A. B. Baggeroer, W. A. Kuperman, and E. K. Scheer, "Envi-

ronmentally tolerant beamforming for high-resolution matched field processing: Deterministic mismatch," J. Acoust. Soc. Am. **88**, 1851–1862 (1990).
[14]J. A. Fawcett, M. L. Yeremy, and N. R. Chapman, "Matched-field source localization in a range-dependent environment," J. Acoust. Soc. Am. **99**, 272–282 (1996).
[15]W. Xu, A. B. Baggeroer, and H. Schmidt, "Performance analysis for matched-field source localization: Simulations and experimental results," IEEE J. Ocean. Eng. **31**, 325–344 (2006).
[16]E. K. Westwood, "Broadband matched-field source localization," J. Acoust. Soc. Am. **91**, 2777–2789 (1992).
[17]J. A. Shorey and L. W. Nolte, "Wideband optimal a posteriori probability source localization in an uncertain shallow ocean environment," J. Acoust. Soc. Am. **103**, 355–361 (1998).
[18]R. Zhang, Z. Li, J. Yan, Z. Peng, and F. Li, "Broad-band matched-field source localization in the East China Sea," IEEE J. Ocean. Eng. **29**, 1049–1054 (2004).
[19]N. C. Makris, "Parameter resolution bounds that depend on sample size," J. Acoust. Soc. Am. **99**, 2851–2861 (1996).
[20]J. A. Fawcett and B. H. Maranda, "Localization accuracies for a moving source in an oceanic waveguide," J. Acoust. Soc. Am. **96**, 1047–1055 (1994).
[21]A. Thode, M. Zanolin, E. Naftali, I. Ingram, P. Ratilal, and N. C. Makris, "Necessary conditions for a maximum likelihood estimate to become asymptotically unbiased and attain the Cramer-Rao lower bound. Part II. Range and depth localization of a sound source in an ocean waveguide," J. Acoust. Soc. Am. **112**, 1890–1910 (2002).
[22]M. Betke and N. Makris, "Recognition, resolution and complexity of objects subject to affine transformation," Int. J. Comput. Vis. **44**, 5–40 (2001).
[23]M. Zanolin, I. Ingram, A. Thode, and N. C. Makris, "Asymptotic accuracy of geoacoustic inversions," J. Acoust. Soc. Am. **116**, 2031–2042 (2004).
[24]I. Bertsatos and N. C. Makris, "Statistical biases and errors inherent in photoclinometric surface slope estimation with natural light," Icarus **208**, 798–810 (2010).
[25]C. R. Rao, *Linear Statistical Inference and Its Applications* (Wiley, New York, 1966), Chap. 5.
[26]O. E. Barndorff-Nielsen and D. R. Cox, *Inference and Asymptotics* (Chapman and Hall, London, 1994), pp. 14–28.
[27]R. A. Fisher, *Statistical Methods and Scientific Inference* (Hafner, New York, 1956), p. 159.
[28]S. M. Kay, *Fundamentals of Statistical Signal Processing: Estimation Theory* (Prentice-Hall, Englewood Cliffs, NJ, 1993), Chap. 3.
[29]L. R. Shenton and K. O. Bowman, *Maximum Likelihood Estimation in Small Samples* (Griffin, New York, 1977), p. 7.
[30]M. Zanolin, E. Naftali and N. Makris, "Second order bias of a multivariate Gaussian maximum likelihood estimate with chain-rule for higher moments," Technical Report No. 13-2003-37, Massachusetts Institute of Technology, Cambridge, MA, 2003.
[31]N. C. Makris, "The effect of saturated transmission scintillation on ocean acoustic intensity measurements," J. Acoust. Soc. Am. **100**, 769–783 (1996).
[32]N. C. Makris, F. Ingenito, and W. A. Kuperman, "Detection of a submerged object insonified by surface noise in an ocean waveguide," J. Acoust. Soc. Am. **96**, 1703–1724 (1994).
[33]S. D., Chuprov, "Interference structure of a sound field in a layered ocean," in *Acoustics of the Ocean: Current Status*, edited by L. M. Brekhovskikh and I. B. Andreevoi (Nauka, Moscow, 1982), pp. 71–91 (in Russian).
[34]L. M. Brekhovskikh and Y. Lysanov, *Fundamentals of Ocean Acoustics*, 3rd ed. (Springer, New York, 2003), Chaps. 5–7.
[35]S. Lee and N. C. Makris, "The array invariant," J. Acoust. Soc. Am. **119**, 336–351 (2006).
[36]C. Soares and S. M. Jesus, "Broadband matched-field processing: Coherent and incoherent approaches," J. Acoust. Soc. Am. **113**, 2587–2598 (2003).
[37]T. Chen, "Mean, variance, and temporal coherence of the 3D acoustic field forward propagated through random inhomogeneities in continental-shelf and deep ocean waveguides," Ph.D. thesis, Massachusetts Institute of Technology, Cambridge, MA (2009).
[38]J. Lighthill, *Waves in Fluids* (Cambridge University Press, Cambridge, 1978), Chap. 4.
[39]A. E. Gill, *Atmosphere-Ocean Dynamics* (Academic, San Diego, 1982), Chap. 6.
[40]W. A. Kuperman and J. F. Lynch, "Shallow-water acoustics," Phys. Today **57**(10), 55–61 (2004).
[41]P. Ratilal and N. C. Makris, "Mean and covariance of the forward field propagated through a stratified ocean waveguide with three-dimensional random inhomogeneities," J. Acoust. Soc. Am. **118**, 3532–3559 (2005).